SPACE TELESCOPE SCIENCE INSTITUTE
Operated for NASA by AURA

Instrument Science Report ACS/WFC 2015-06

ACS/WFC Revised Geometric Distortion for DrizzlePac

V. Kozhurina-Platais, D. Borncamp,

J. Anderson, N. Grogin, W. Hack

June 29, 2015

Abstract

The goal of the ACS/WFC astrometric calibration for DrizzlePac is to provide a coordinate system free of distortion to a precision level of ∼0.1 pixels (∼ 5mas). The astrometric calibration of ACS/WFC is based on the astrometric standard field in the vicinity of globular cluster 47 Tuc. We used a polynomial model to derive the geometric distortion in the WFC channel relative to the distortion–free coordinates, which now accounts for proper motions of stars in the astrometric field. A new and straightforward representation of time-dependent distortion in the linear terms is now implemented in the IDCTAB reference file and in the STScI software DrizzlePac to obtain simultaneously the ACS/WFC geometric distortion and its time-dependent correction. As a result, the geometric distortion can be corrected down to a precision level of 0.02 pix (1mas), which allows now for improvement of the alignment and registration of the ACS/WFC images with accuracy of ∼0.05 pix (2.5mas) or better.

1. Introduction

It is well-known that the HST imaging instrument ACS/WFC has a considerable geometric distortion due to the optical assembly of the telescope. By design, the focal plane of

the ACS/WFC camera is tilted with respect to the incoming beam at $\sim 28^{\circ}$ and as a result the images are distorted by up to $\sim 11\%$ across the detector. This distortion, in the form of displacement of celestial sources from their true positions on the sky, can reach up to $\sim$120 pixels ($\sim 6''$). Knowledge of accurate geometric distortion is important not only for deriving accurate positions, parallaxes and proper motions of the scientifically interesting objects but also to rectify the ACS/WFC images and to stack and combine multiple exposures of the dithered ACS/WFC images into a common frame. The STDAS DrizzlePac[1] software (Gonzaga et al., 2012), currently installed in the STScI on-the-fly pipeline (OTFR), requires an accurate distortion correction in order to combine the dithered ACS/WFC images, to reject cosmic rays, to enhance the spatial resolution, and to deepen the detection limit. Any significant uncertainty in the geometric distortion correction is therefore detrimental to the alignment of ACS/WFC images with DrizzlePac software and to mitigating the effect of under-sampled PSF.

The knowledge of geometric distortion coefficients is fundamental not only for use by DrizzlePac, but also on-the-fly calibration in the HST pipe-line (OTFR) in order to remove the distortion from HST (`*_flt.fits`) images. These geometric distortion coefficients are stored in a reference file, called Instrument Distortion Coefficients Table (IDCTAB, Hack & Cox, 2001), which is in the HST V2&V3 coordinate system (equivalent to the sky tangential-plane). The ACS/WFC geometric distortion coefficients derived by Anderson (2002) were obtained by a self-calibration technique using the first images right after installation of the ACS camera in 2002. These coefficients are in the detector coordinate system. In order to put them into the IDCTAB (V2&V3 system), the geometric distortion coefficients from Anderson were transformed by scaling, shifting and rotating them into the official Meurer solution (2002), which were in the HST V2&V3 system. Since 2002, the current ACS/WFC IDCTAB, based on the Anderson and Meurer solutions has been used in the HST pipe-line and by the improved STSDAS software DrizzlePac.

In cases demanding very high accuracy of the astrometric alignmnet (such as UDF, Frontier Fields), this original solutions are not adequate. In addition to large geometric distortion, ACS/WFC also has a time-dependent distortion. Shown by Anderson (2007), the X&Y scales, presented by linear terms in the ACS/WFC geometric distortion, have changed monotonically since the ACS was installed in 2002. The size of this change is clearly noticeable over 5 years, reaching about 15 mas (0.3 pixel) off from the original 2002-based distortion solution. This level of systematic trend in the ACS/WFC distortion model introduces a poor alignment ($\sim$ 0.2 pixel) of drizzled ACS/WFC images with MultiDrizzle

[1]http://drizzlepac.stsci.edu

in the past and as well with new DrizzlePac software. After the Servicing Mission 4 (SM4, May 2009), the linear distortion terms have significantly changed, as described by Bedin & Smith (2010). The full analysis and calibration of the time-dependents of the linear terms in the geometric distortion after SM4 are described by Ubeda *et al.* (2013), following the approach by Anderson (2007) and Bedin & Smith (2010). Summarizing, the time-dependent distortion (TDD) calibration and its correction include: *(i)* linear parameters of TDD derived and analyzed from X&Y positions already corrected for distortion which are in the detector coordinate system; *(ii)* linear parameters of TDD applied in addition to X&Y positions already corrected for distortion. This empirical correction for time-dependent distortion ensures the level of 0.02 WFC pixel (1 mas) in the global astrometric ACS/WFC accuracy.

The original TDD correction is in the X&Y detector coordinates system. However, IDCTAB is on the system of HST V2&V3 coordinate system, thus the TDD correction has to be converted into the V2&V3 system. It is not trivial to transform the linear parameters of the TDD fit from one coordinate system into another; it required complicated numerical manipulation of the IDCTAB parameters. As a result, the linear terms in the IDCTAB introduce uncertainties in the geometric distortion correction and lead to the poor alignment ($\sim$ 0.2 pix) of ACS/WFC images and HST cross-instrument alignment (*e.g.* ACS/WFC and WFC3 images). Thus, the ACS/WFC geometric distortion should be re-calibrated, in order to provide more accurate, precise and stable distortion to use in the STScI on-the-fly pipeline (OTFR) and STDAS *DrizzlePac* software.

Successful WFC3 geometric distortion calibration (Kozhurina-Platais, *et al.* 2009a, 2009b) allows us to consolidate the past experience in order to improve the long-standing issue of the ACS/WFC geometric distortion. While WFC3/UVIS and ACS/WFC are different instruments, many problems involved in the astrometric calibrations are applicable for the ACS/WFC geometric distortion calibration. For the geometric distortion calibration of the WFC3/UVIS and IR, the standard astrometric catalog was used (Kozhurina-Platais *et al.* 2009a,b) which is a straightforward way to solve for accurate polynomial coefficients of geometric distortion. The accurate and precise positions of the standard astrometric catalog were instrumental in revealing systematics in the X&Y raw measured positions from WFC3/UVIS exposures. Particularly, it led to the discovery of CCD pixel-grid irregularities due to the lithographic-mask pattern in the WFC3/UVIS detector (Kozhurina-Platais *at al.* 2010). In addition, the imperfections in the WFC3/UVIS filters causes fine-scale distortion variations in each filter and complicates the structure of X&Y residuals after removing geometric distortion. Therefore, all this previous experience is used here in the revised ACS/WFC distortion.

The aim of this report is three-fold. First, we provide a short description of the standard

astrometric catalog and the proper motions that have been computed for it. Second, we give a detailed account of the geometric distortion model and all the steps leading to a high accuracy distortion correction. Finally, we describe the implementation of the geometric distortion coefficients in the IDCTAB to be used in OPUS and DrizzlePac.

2. Standard Astrometric Catalog

The straightforward way to solve for distortion is to compare the positions of stars in the detector coordinates with the positions of the same stars in an "astrometric standard catalog", where the star positions are free of distortions. The residuals between the observed positions of stars and the corresponding positions in an astrometric standard catalog then reveal the geometric distortion directly. In the case of the *ACS/WFC* detector, besides the expected non-linear distortion there is also a considerable linear distortion. According to Anderson (2007), these linear distorion are known as two kinds of the skew terms, which manifest as a departure from non-orthogonality between the two principle axes and as a scale difference between two principal axes. Neglecting the linear distorion, a nearly square WFC detector will be projected onto the sky in a rhombus shape rather than a square. For such a complicated model of the optical distortion in *ACS/WFC*, a high precision astrometric standard catalog is fundamental to derive an accurate and complete characterization of geometric distortion.

2.1. Reference Frame

The reference frame, based on all existing ACS/WFC observations of 47 Tuc from 2002 to 2006 through F606W filter, was constructed by Anderson (2007). The tangential-plane positions of stars in this catalog are given at the average epoch of 2004.5 and are accurate to ∼0.02 ACS/WFC pixel (0.1 mas) across of the entire catalog (Anderson, 2007). A great number of ACS/WFC images with different range of offsets and orientations were used to create the master list of stars positions. These positions were were stacked into a non-photometric but representative image of the field, at α=$00^h22^m35\overset{s}{.}0$ & δ=-72°04′00″ at frame coordinate corresponding to pixel (5000,5000). Figure 1 shows a stacked image made from all ACS/WFC exposures of 47 Tuc. Since all 47 Tuc observations were taken at about 6.7′ West from the center of this globular cluster, there is strong evidence of the gradient stellar radial density profile. As seen in Figure 2, stars are more concentrated toward the center of the cluster on the East side. However, despite this gradient there are sufficient number of stars in all parts of the field to permit an accurate calibration of the ACS/WFC geometric

distorion.

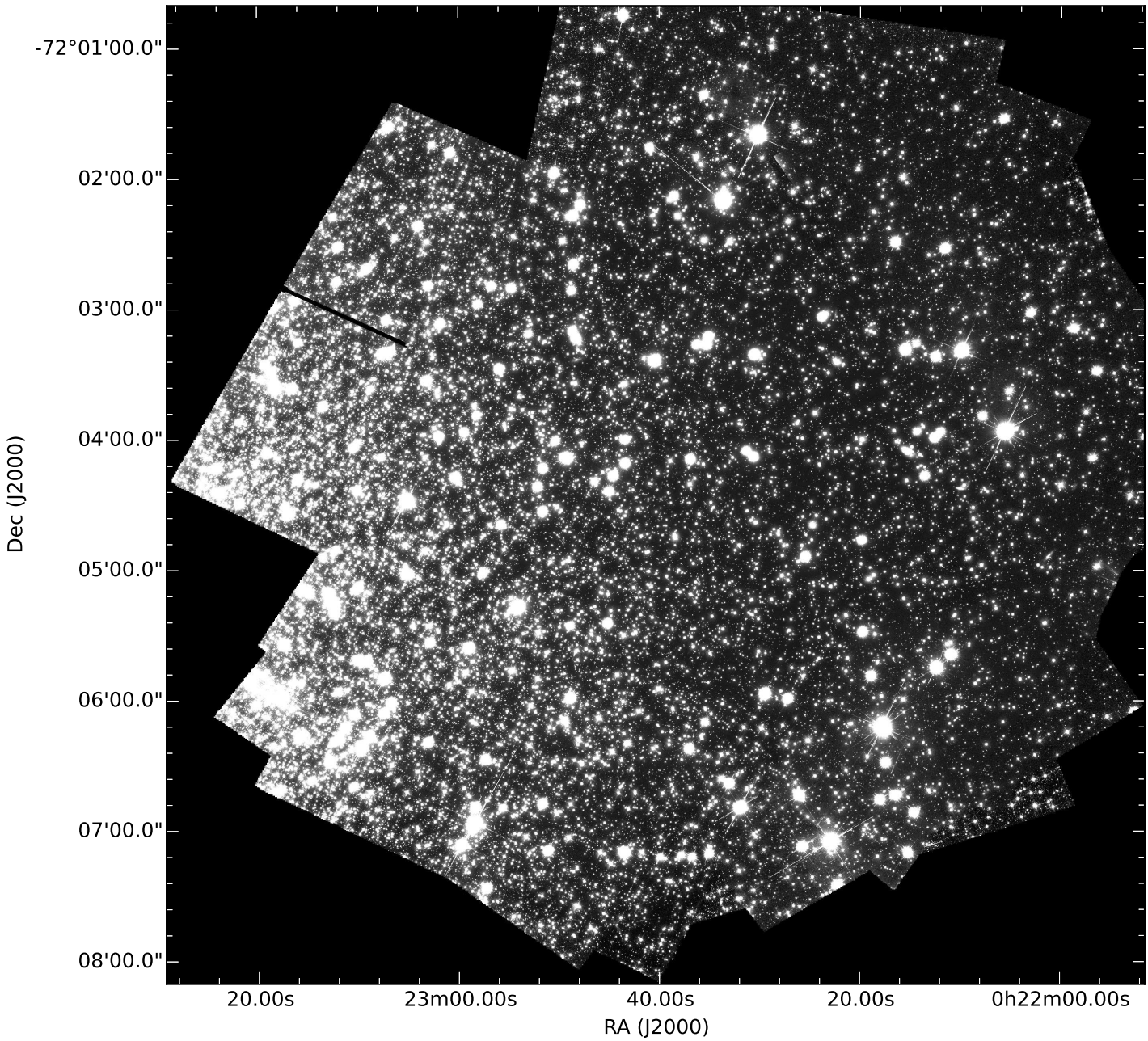

Fig. 1.— Stack of all ACS/WFC F606W images used to create the master star list.

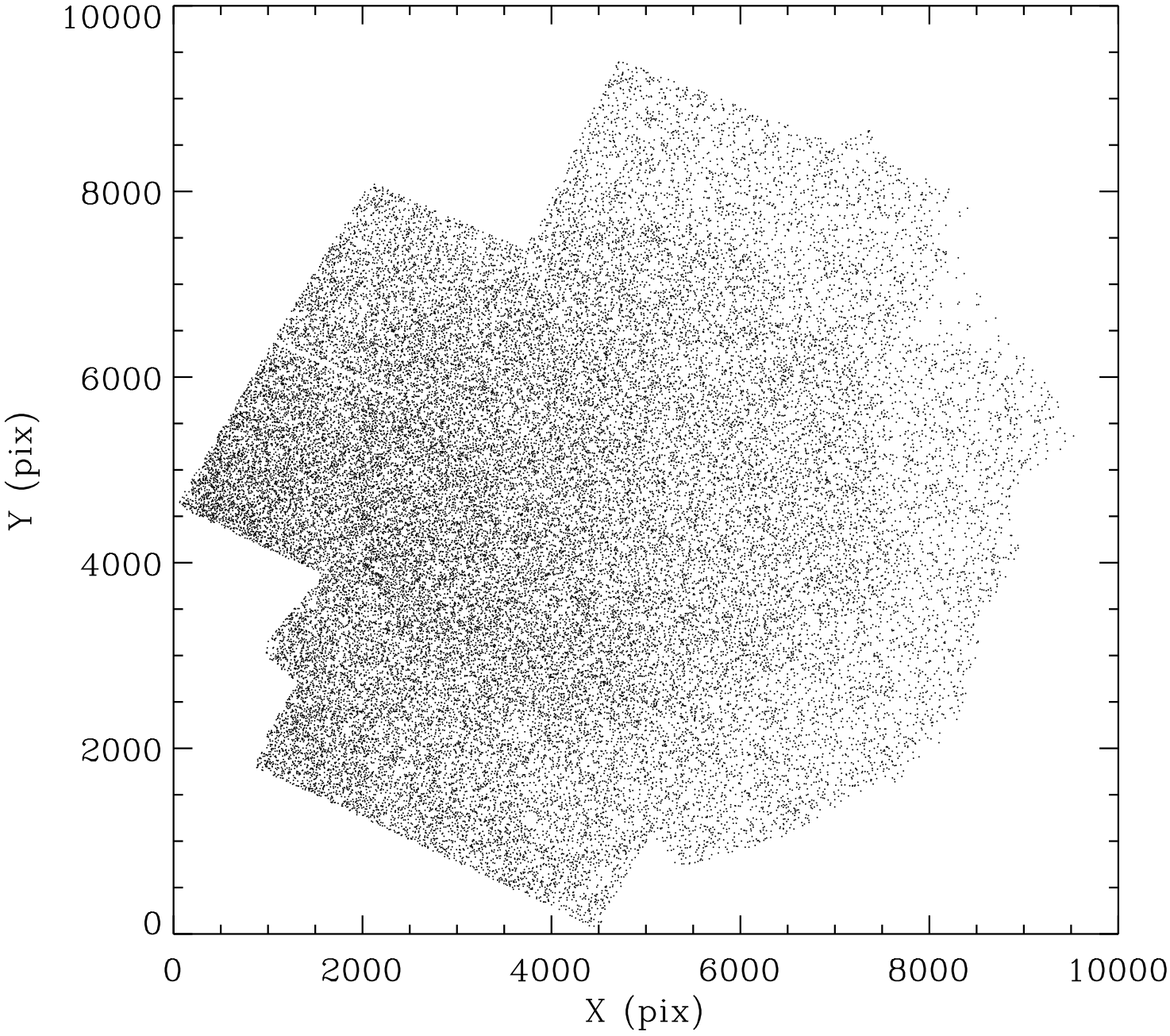

Fig. 2.— X&Y positions of 53917 well–measured stars in the master star list. The X and Y coordinates are given in ACS/WFC pixels.

2.2. Proper Motions

Stars in globular clusters are all moving, and the internal velocity dispersion in proper motions of 47 Tuc is at the level of ∼0.01 pix/yr in each coordinate, according to Anderson (2007). As the average epoch of the reference frame provided by Anderson (2007) is 2004.5, the positions in this reference frame are degrading over time. For example, an epoch difference of 4 years contributes to the degradation of X&Y positions as much as 0.04 pixel or more. For this reason, the astrometric catalog in the vicinity of 47 Tuc based on epoch 2004.5 positions has to be updated, taking into account the motions of stars.

In order to calculate the propoer motions, the observations of 47 Tuc taken through F606W filter were divided between those obtained before and after SM4 (2009-2014). An averaged posistion for each star were obtained in the pre-SM4 data along with the average epoch in which it has observed. Similarly, an averaged position for each star were obtained in the post-SM4 data. The proper motions were then determined from the difference between the average pre-SM4 and post-SM4 positions divided by the time difference of the two average positions. The left panel in Figure 3 shows the formal errors of the X&Y measured positions as function of the ASC/WFC instrumental magnitude ($Inst.mags = -2.5log(\frac{Flux}{Exp.Time})$). The right panel in Figure 3 shows the proper motion error in both coordinates as a function of ACS/WFC instrumental magnitude.

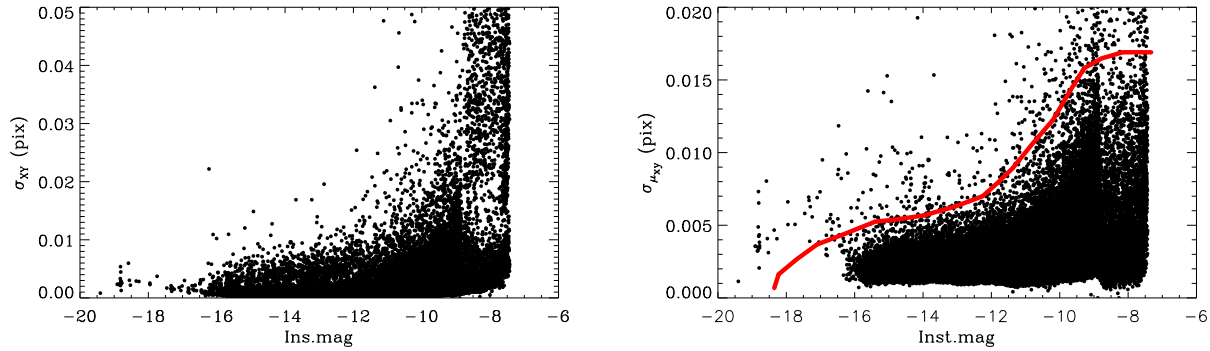

Fig. 3.— Left Panel: Formal centering errors of X & Y positions as a function of instrumental magnitude, for stars in the master catalog. Positional errors (σ_{XY}) are calculated as $\sqrt{(\sigma_X^2 + \sigma_Y^2)}$. Right Panel: Proper motion errors as a function of instrumental magnitude. Stars with proper motion errors above the red line are poorly–measured.

As seen in the left panel of Figure 3, the formal centering errors for well measured stars (Inst.mag $\lesssim$-10) are less than 0.02 pixel in each coordinate. Stars with proper motion errors above the red line in Figure 3 right panel were not used in the analysis of geometric distortion solutions. Thus, a total of 49647 well-measured stars out of 53917 stars from the standard astrometric catalog were used for calibration of the ACS/WFC geometric distortion.

3. Observations and Reductions

The outer field of globular cluster 47 Tuc has been observed repeatedly over 13 years with ACS/WFC on board HST. The F606W ACS/WFC filter was chosen as a reference filter for geometric distortion calibration since it has hundreds of observations not only for the purpose of ACS/WFC calibration but also for science projects (*e.g.* GO-11677, PI– H. Richer). From all available observations of 47 Tuc we selected images that are fully over-lapping with the standard astrometric catalog and equally distributed in time over the 13 years of observations and cover the full range of HST roll angle (PA_V3), yielding a total of 110 representative images. Figure 4 shows footprints of all selected images used for calibration of geometric distortion imposed on the standard astrometric catalog. As seen in Figure 4, the selected images have different orientations, pointings, and they cover well the entire field of standard astrometric catalog.

The precision of geometric distortion calibration also depends on the accuracy of measured pixel positions from each individual ACS/WFC image. Therefore, a key in the analysis of geometric distortion is to measure accurate and precise positions of each star in each CCD chip and in each exposure. One of the uncertainties in measurements of X&Y positions is the effect of Charge Transfer Efficiency (CTE). It is a known fact that the CTE of the ACS/WFC detector has been declining over time as on-orbit radiation damage creates charge traps in CCDs. The CTE losses introduce not only a loss of flux but also a centroid shift, the amplitude of which depends on a star signal level and its position on the CCD chip (Kozhurina-Platais *et al.*, 2007). CTE-induced centroid shifts in X&Y positions are typically on the order of $\sim$0.1 pixel, and are increasing with time. This amount of centroid shifts is significant for high-precision astrometry. To correct for the CTE-induced centroid shift, all selected observations were processed through the pixel-based CTE correction (Anderson & Bedin, 2010) algorithm.

The accuracy of measured X&Y positions also depends on the accuracy of the PSF model representing the ACS/WFC PSF which is under-sampled and varies across the CCD chips. Because of that, the actual ACS/WFC PSF may suffer from systematic errors, which in turn affect the positional measurement of a star, depending on its location on the chip.

Anderson & King (2000) developed a purely empirical model (the effective PSF or ePSF) to describe the PSF of WFPC2 and perform high–precision photometry and astrometry from WFPC2 images. In 2002, they extended this model to ACS/WFC (Anderson & King 2006) and represented its spatial variations with an array of 9×5 fiducial PSFs across each ACS/WFC CCD. The routine img2xym_WFC.09x10.F uses these ACS/WFC ePSFs to find and measure stars in images. Only the central 5×5 pixels are fit with the local PSF to determine a position and flux for each star. The output from this routine is a list of high-precision X&Y raw positions, the distortion–corrected X&Y positions (accurate to the level of 0.01 pixel), flux and the quality parameter q of PSF fit (the residuals to the PSF fit) for each star from each ACS/WFC image. Figure 5 shows the typical instrumental ACS/WFC magnitude ($Inst.mags = -2.5log(\frac{Flux}{Exp.Time})$ were) versus the quality of PSF fit. The stars brighter than −14 instrumental magnitude are saturated; that is why quality of the PSF fit becomes very poor. For well–measured stars with $-14 \lesssim$ Inst.mag. $\lesssim -10$, the quality of a PSF fit is less than 0.02 in each coordinate.

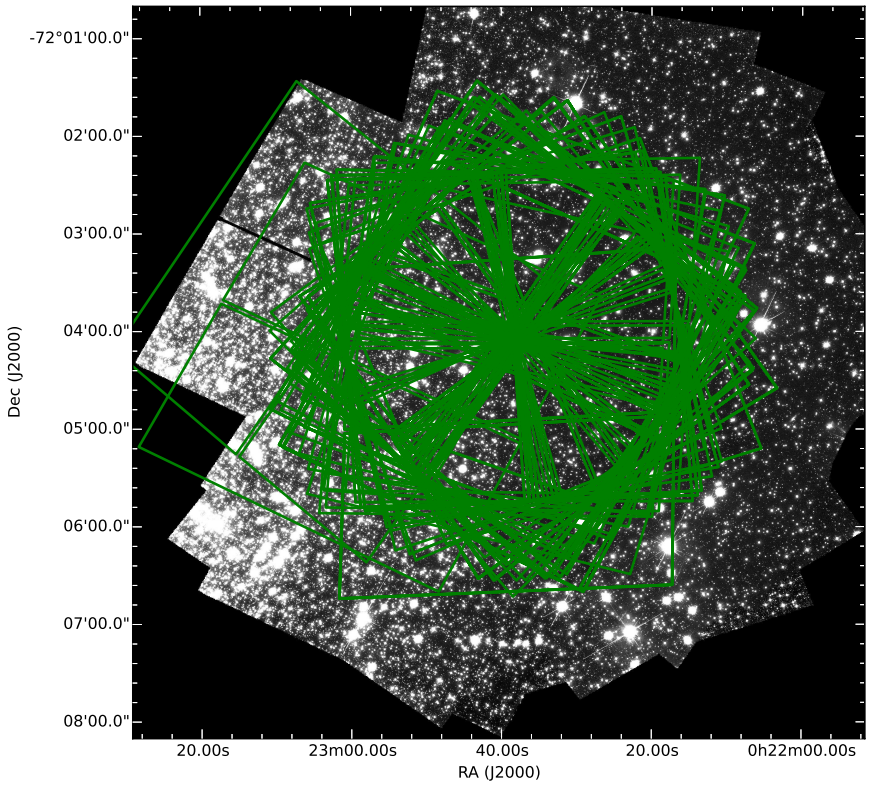

Fig. 4.— Footprints of 47 Tuc observations used for the geometric distortion calibration over-plotted on the stack image of standard astrometric catalog.

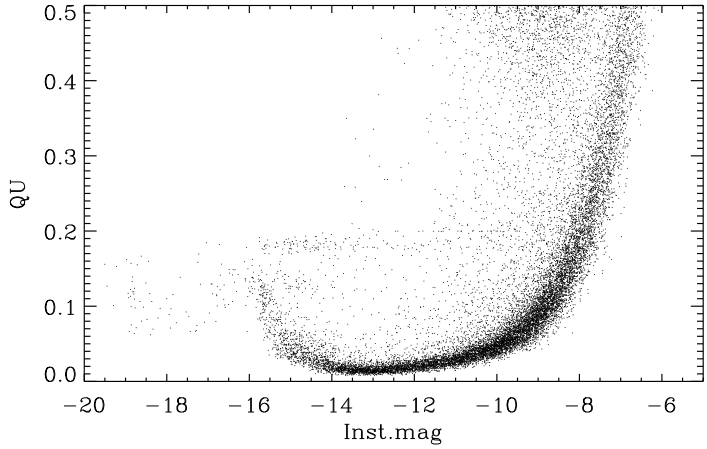

Fig. 5.— Quality of PSF fit as a function of instrumental magnitude for all stars found in ACS/WFC image The stars brighter that about −14 instrumental magnitude are saturated. Star with instrumental magnitude $\gtrsim -14$ are well–measured and the quality of fit is lees than 0.02 in each coordinate.

4. Geometric Distortion Solution

4.1. Matching the Stars

The first step in solving for distortion is to match the measured positions of stars from ACS/WFC images with the same stars in the astrometric standard frame. This is not an easy task due to the arbitrary orientation of the ACS/WFC images. It would be much easier to use the sky positions, RA and Dec of the astrometric standard catalog and compare them with calculated RA and Dec from the header World Coordinate System (WCS) information of ACS/WFC image. However, we want to avoid using the WCS information from the header as much as possible. First, we wish to reach the accuracy and precision of the original pixel coordinates. Second, the maximum precision is preserved only if all data manipulations are performed with the original pixel coordinates. And third, the transformation from one coordinate system to another may introduces model-dependent systematics, also known as a modeling error, depending on how complicated the transformation is. To our benefit, ACS/WFC geometric distortion is already reasonably well known from early calibration by Anderson (2002). Thus, X&Y positions corrected for this known distortion are used to match the stars in each exposure with catalog positions, employing the linear transformation in the least-squares minimization (shift, scale and rotation) to find the common reference stars

for each ACS/WFC CCD chip, interactively rejecting poorly–measured, saturated stars and cosmic rays. During the matching procedure, the catalog positions were updated for proper motions to the epoch of the observed frame. The output from this matching procedure is a list of reference stars with original full-precision X&Y raw pixel positions of stars from the observed frame and the updated positions from the astrometric standard catalog. In addition to astrometric positions, there is also instrumental magnitude for each star from each observed frame and corresponding averaged magnitude from the standard astrometric catalog.

4.2. The Model of Geometric Distortion

After measured stars from the ACS/WFC images were matched to the same stars in the astrometric standard catalog, we proceeded with the solutions for geometric distortion.

The general form of geometric distortions is a polynomial containing all terms up to the 5th-order, as follows:

$$U = A_1 + A_2X + A_3Y + A_4X^2 + A_5XY + A_6Y^2 + A_7X^3 + ... + A_{21}Y^5 \quad (1)$$

$$V = B_1 + B_2X + B_3Y + B_4X^2 + B_5XY + B_6Y^2 + B_7Y^3 + ... + B_{21}Y^5 \quad (2)$$

where U and V are the tangential-plane positions in the astrometric standard catalog, and X,Y are measured pixel positions in the observed ACS/WFC frame. An examination of various terms in Eqs. (1) and (2) helps to illustrate the strategy of finding the distortion correction. If the (U, V) and (X, Y) systems are well aligned, then, for example, in the X solution: A_1 is an arbitrary offset between the two coordinates systems, A_2 and B_3 is the relative plate scale, A_4 and A_5 are plate tilt terms (van de Kamp, 1967), A_7 through A_{21} are classical cubic- and fifth-order distortion terms, respectively. If the centers of the two coordinate systems are not properly matched, and/or there is rotation between the two frames, the quadratic and 4th order terms will be nonzero. Thus, a key to determine the geometric distortion is to find a good alignment between two coordinate systems.

In order to properly align the two coordinate systems ACS/WFC $X\&Y$ pixel and $U\&V$ astrometric standard catalog, we made the following assumptions:

- WFC CCD chip 2 (WFC2) was chosen as a basic reference frame and its X-axes as a primary reference axes because of the presence of large skew term in WFC CCD chips;

- zero-point of each WFC CCD chip is adopted at $X = (x-2048.0)$ and $Y = (y-1024.0)$, where x and y are measured positions from each chip, assuming that all geometric distortions are zero only at this specific point;
- WFC2 must be rotated and shifted so that there is zero offset in X & Y between WFC2 and the astrometric standard catalog and there is no rotation between the X-axis in both systems.

In order to put these assumptions into practice, the nearest star to the center of the WFC2 CCD chip was used to find the initial offsets and the rotation center of the astrometric standard. The final offsets, the location of the rotation center, and the amount of rotation are obtained through iterative least-squares solutions and successive small adjustments to the offset/rotation parameters. This process of minimization is non-trivial because of a skew between the X and Y axis. In order to account for this, we chose the X axis as a reference with respect to which there is no rotation, *i.e.* minimizing the ratio of linear terms A_3/B_2. The U and V positions of the stars from the astrometric standard, matched to the X and Y positions from WFC2, were rotated with respect to the center of WFC2, thus eliminating rotation between the WFC2 X-axis and the U-axis of the astrometric standard.

Once the rotation center and the X & Y offset between WFC2 and the standard astrometric catalog are found and rotation eliminated, a new full least-square solution is performed which includes all necessary high-order polynomial terms. This solution constitutes the geometric distortion for WFC2.

After the geometric distortion is solved for WFC2, we can solve it for the other CCD chip WFC1. However, the presence of the inter-chip gap complicates the task of finding the geometric distortion solution for WFC1 CCD chip. Similar to WFC3/UVIS inter-chip gap, it requires a single geometric solution, so, that measured X & Y positions corrected for distortion could assembled be into a single coordinate system.

The united geometric distortion solution is fully described by Kozhurina-Platais *et al.* (2009a), where the meta-chip solution is similar to the meta-chip geometric solution by Anderson (2002). The key point here is that simultaneously with WFC2 we shifted and rotated the matching astrometric standard coordinates for WFC1 as well. As described above, the astrometric standard frame in WFC2 is rotated about the central point by the angle required to align the U-axis to the X-axis at that point. At the same time we relate X,Y on WFC2 and X,Y on WFC1 to the same astrometric standard frame in WFC2. In this way, we achieve the meta-chip configuration for both chips *simultaneously* and directly into the system of our reference chip WFC2. A straightforward least-squares solution provides the coefficients of geometric distortion for WFC1 in the same system as for WFC2. Thus, the

meta-chip gap and rotation between the two chips is now implicitly included in the geometric distortion coefficients.

After the polynomial coefficients of Eqs.1-2 were derived from each exposure or each individual solution, each coefficient of Eqs.1-2 was examined by its value and the formal error, as returned by a least squares minimization. Careful analysis of the polynomial terms in each solution led us to the conclusion that all terms – linear, quadratic and classical distortion terms are consistent from one solution to another and significant with respect to their errors, except for the fifth-order, which are very small (on the order of 10^{-17}) and vary from one solution to another. In the final geometric distortion solution, for each ACS/WFC CCD chip is represented by a fifth-order polynomial.

Figure 6 shows the positional residuals between the 47 Tuc ACS/WFC observed frame and the standard astrometric catalog after applying the best polynomial fit. As seen in Figure 6, the large–scale residuals due to the optical distortion are largely removed. Nevertheless, there appears to be noticeable fine-scale systematic residuals from the best–fit polynomial solutions, showing clearly elongated distribution of residuals, especially for WFC1.

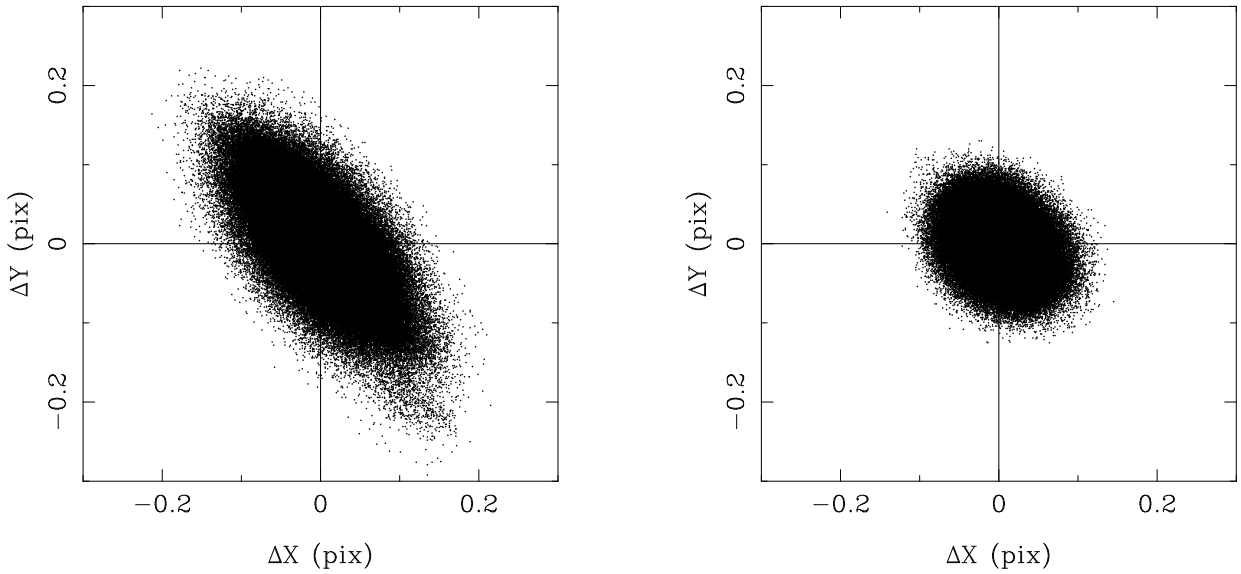

Fig. 6.— XY-residual plot between an observed frame and the standard astrometric catalog after the best-polynomial solutions. The left panel shows the residuals plot from WFC1 CCD chip. The right panel shows the positional residuals plot from WFC2 CCD chip. The units are ACS/WFC pixels..

4.3. Fine-Scale Distortion

In order to investigate the nature of such an odd distribution of residuals, we evaluated their spatial distribution. Figures 7, 8, and 9 show binned after the best-polynomial solution X&Y residuals in the form of vector diagrams for 3 selected ACS/WFC filters, F606W, F475W and F435W. Complicated and correlated structure of these residuals is similar between various ACS/WFC filters, with significant correlated and stable pixel grid irregularities in both ACS/WFC CCD chips, which can reach ∼0.2 pixels in amplitude across the ACS/WFC FOV. This is an indication that the irregularities in the pixel grid actually are imprinted onto the detector itself during the manufacturing process of CCDs.

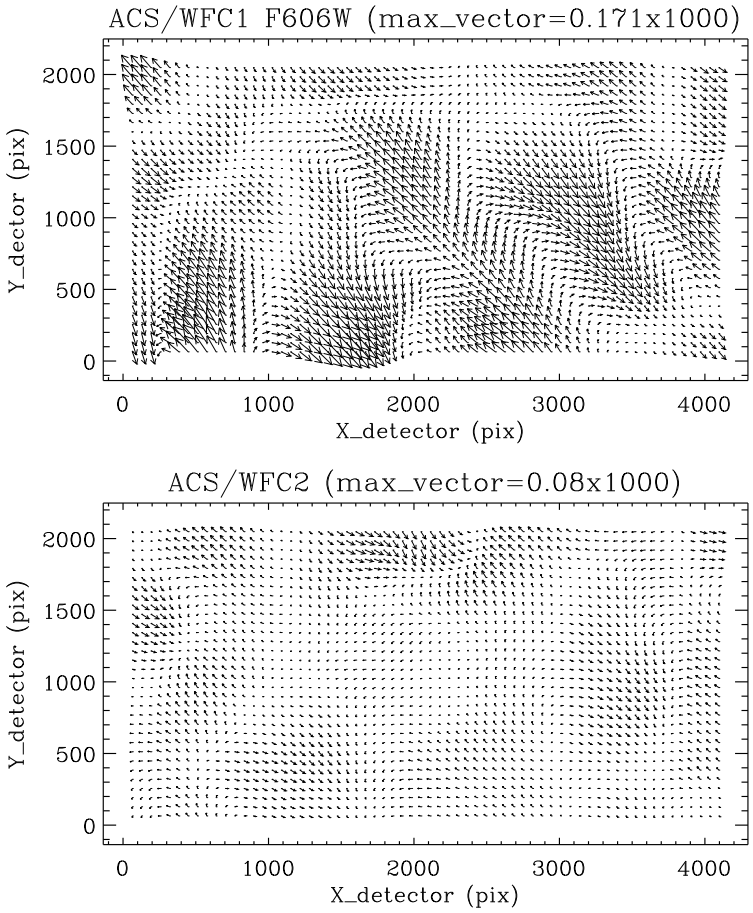

Fig. 7.— Binned XY-residual map between F606W observed frames and the standard astrometric catalog after the best polynomial solution. The top panel shows the WFC1 CCD chip. The bottom panel shows WFC2 CCD chip. Each vector is magnified by 1000. The units are ACS/WFC pixel.

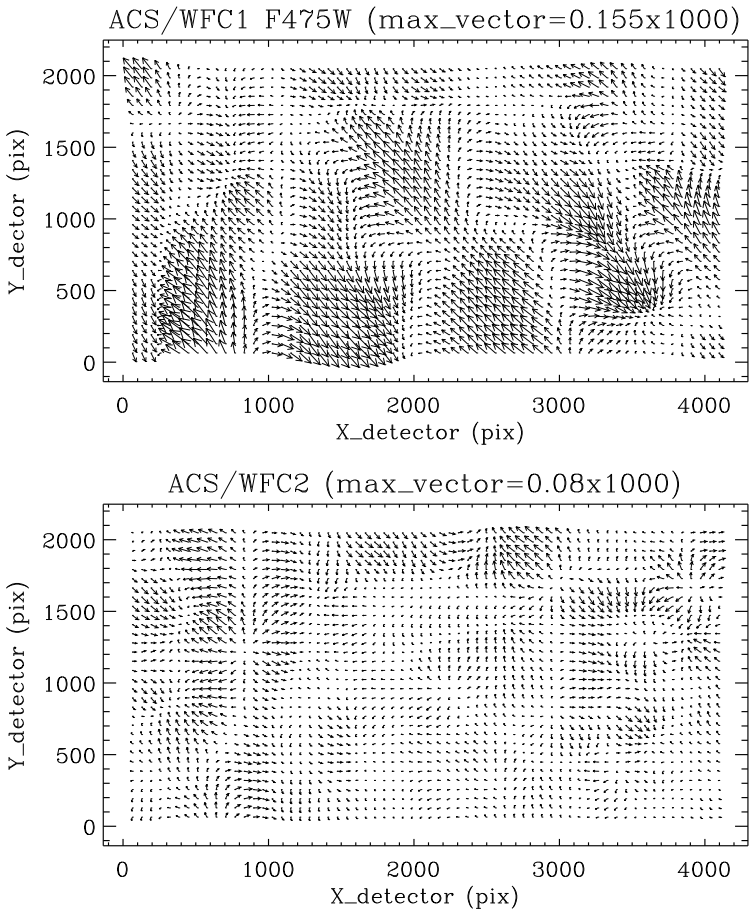

Fig. 8.— The same as Figure 7 only for F475W filter. The units are ACS/WFC pixel.

These fine-scale systematic residuals typically extend to $\sim$ 0.2 pixel and vary in amplitude depending on the location within the WFC1 CCD chip. On the other hand, for the WFC2 CCD chip, the maximum amplitude of vector is 2 times less and the pattern in variation across the chip is different. The different pattern in fine-scale systematic residuals in ACS/WFC chips suggests that each CCD chip probably went through a different manufacturing process. We conclude that, these fine–scale and low–amplitude distortions are the result of: (1) a detector flaw caused by the manufacturing process and (2) imperfections in the individual filters. The origin of this effect is not yet well understood (D.Golimowski & M. Sirianni, private communication). For example, in the case of WFPC2, a small manufacturing defect occurs at every $\sim$34th row of each of the WFPC2 chips (Anderson & King, 1999). This defect introduced periodic errors in astrometry at $\sim$ 0.03 pixel level. In the case of the ACS/WFC, a similar detector defect was identified in every 68th column, which induces a periodic error in astrometry of $\sim$ 0.1-0.8% (Anderson, 2002). For both WFPC2

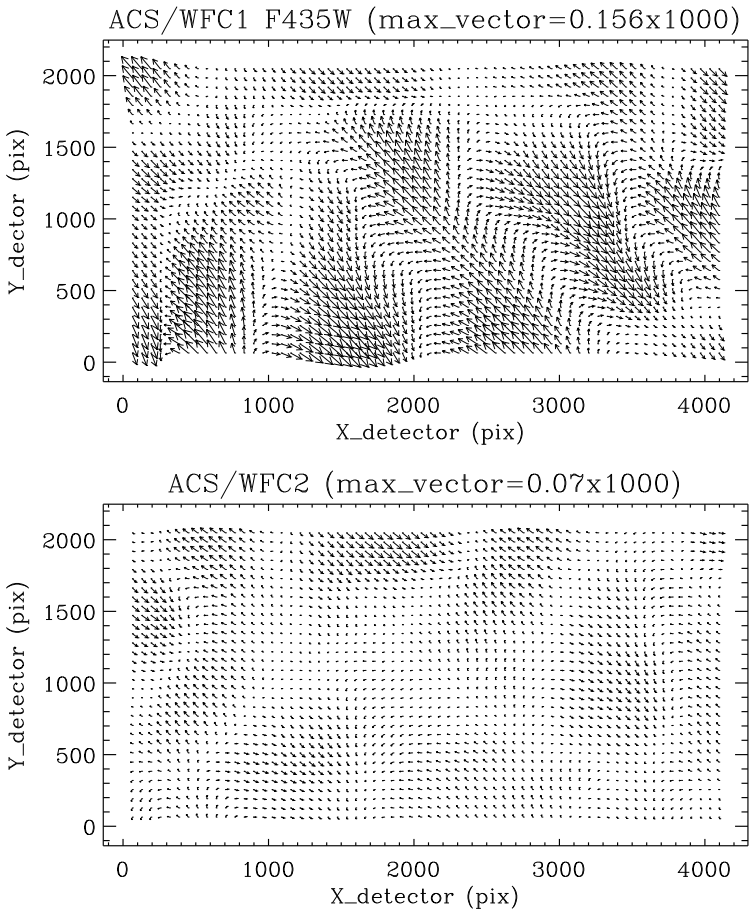

Fig. 9.— The same as Figure 7 only for F435W filter. The units are ACS/WFC pixel.

and ACS/WFC, the detector defect is presented as a 1–D look-up table correction, in either the X or Y direction. In the case of WFC3/UVIS, the pixel-grid irregularities are due to the lithographic-mask pattern imprinted onto the detector itself (Kozhurina-Platais, *et al.* 2010, 2013, 2014). The WFC3/UVIS lithographic pattern is also described by Bellini *et al.* (2011), although the detector defect (lithographic-pattern mask) correction has not been separated from the fine-scale distortion in the filter.

As seen in Figure 7, the F606W filter appears to show a smoother residual map than the F475W, for example. Smaller and less complicated structure in the F606W residuals map is an indication of smaller irregularities in the filter itself. Because of this, the F606W filter has been chosen as the base for the pixel grid irregularities distortion solution while the other filters are essentially tied into the F606W filter.

4.3.1. ACS/WFC Pixel-Grid Irregularities

As discussed by Kozhurina-Platais (2014), in the case of the WFC3/UVIS lithographic-mask pattern the complicated structure of irregularities in the pixel grid cannot be modeled by high-order polynomial. A simple way to remove this patten of fine-scale variations in X&Y raw positions across the CCD detector is to construct a look-up-table, which then can be linearly interpolated at any point in the ACS/WFC images. Since the detector defect is filter independent, this correction must be applied first to the raw X&Y ACS/WFC positions, prior to the large-scale distortion (polynomial model) correction and before considering a filter-dependent correction. Thus, we constructed a separate look-up table to deal only with the detector-defect correction. The computed residuals of X and Y positions from the best polynomial solutions in the F606W filter were used to construct the initial look-up table. There are a couple of restrictions on the structure of such a look-up table:

- it should accommodate the format limitations imposed by DrizzlePac software and the STScI on-the-fly pipeline;
- it should optimize extraction of the 2-D detector defect structure over both ACS/WFC CCD chips;

Here, we adopted the technique used to correct the WFC3/UVIS lithographic-mask pattern by Kozhurina-Platais (2014). Following this approach, a 64×64-pixel bin size has been imposed over the entire 4096×2048 pixel residual map of each ACS/WFC CCD chip. This bin size is chosen to accommodate the format limitations which comply with the constraints of the DrizzlePac software and the STScI on-the-fly pipe-line. The numerical implementation was realized in FORTRAN code binning residuals over an array of 64×32 points per CCD chip. The binned data are first averaged with iterative sigma-clipping. Then, each grid point of residuals is smoothed with a 5×5 quadratic kernel (Anderson & King, 2000).

Applying the newly–derived look-up table of the ACS/WFC irregularities pixel-grid correction to the raw X&Y positions, and then correcting them for the improved polynomial coefficients of geometric distortion, the vector plot of residuals in F606W filters is now free of any systematics (Figure 10). There is no indication of the pixel-grid irregularities pattern or any other spatial structure. The residual map looks smooth, and the RMS scatter of residuals is reduced down to ∼0.03 pixels. The improvement is significant; the largest vector before correction is ∼ 0.17 pixel (Fig.7), and after the correction the largest vector is reduced ∼5 times. The remaining fine-scale systematics with a coherence scale of ∼100 pixels has a typical amplitude of 0.03 pixel which are mostly small irregularities in the F606W filter itself.

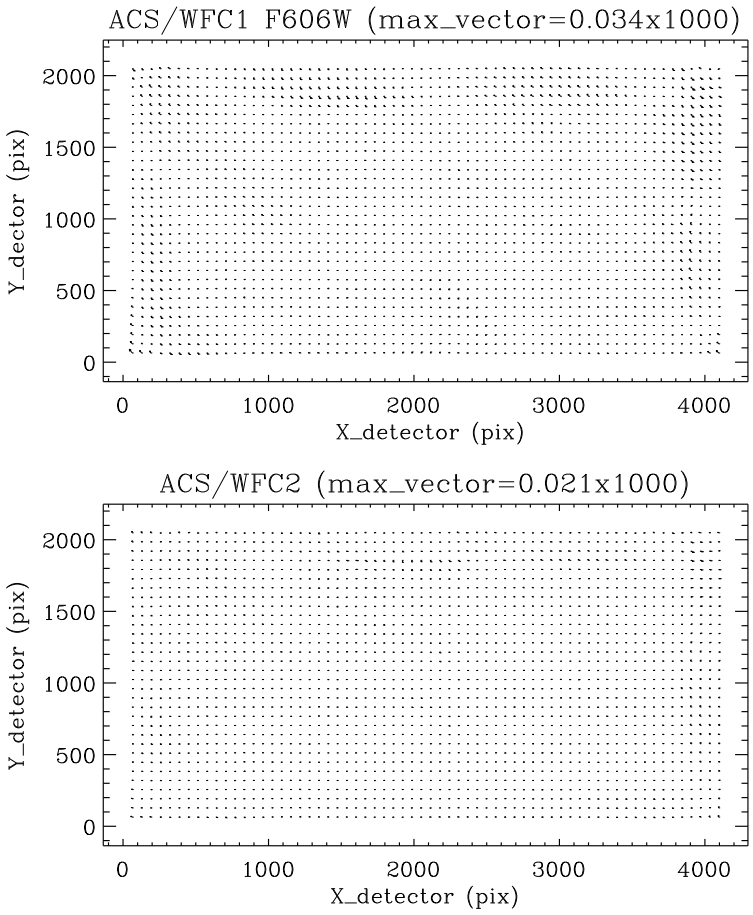

Fig. 10.— The same as Figure 7 but after the correction of X&Y raw positions in F606W filter for the pixel-grid irregularities. The largest vector is ∼0.03 pixel, magnified by factor of 1000. Units are ACS/WFC pixels.

The final look-up table correction derived from observations taken through the F606W filter was used to correct the X&Y raw positions of other ACS/WFC filters. After applying this new correction, new geometric distortion solution was generated for each of the ACS/WFC filters, yielding a new set of improved polynomial coefficients for the ACS/WFC geometric distortion.

4.3.2. Non-Polynomial Filter Dependent Distortion

After applying the correction for the pixel-grid irregularities to X&Y raw positions, and the best polynomial fit, the residuals map between ACS/WFC positions and the reference catalog still shows a complicated fine-scale structure of systematic errors across both ACS/WFC CCD chips. The amplitude of these residuals varies from ∼0.02 to ∼0.05 WFC pixels and the overall pattern of residuals is different for different filters. This is an indication of the filter-dependent component of distortion due to their manufacturing process. It would require a high order polynomial (up to 15th and higher) to remove it, which would be inconvenient and complicated. The smoothing technique as described above (Sec.4.3.1) was used again to obtain a 2–D look-up table correction for each ACS/WFC filter. Examples of resulting smoothed maps of filter-dependent correction are shown in Figures 11-13. An iterative approach is required to improve the filter-dependent distortion correction and simultaneously to improve the polynomial coefficients of geometric distortion. As a result, the systematic errors in the residual are reduced from ∼0.05 pixel down to ∼0.02 pixel, depending on the filter. Figures 11-13 (right panels) show a 2–D map of the X&Y residuals between the positions in ACS/WFC filters and the standard catalog after correction for pixel grid irregularities, filter-dependent distortion & improved polynomial geometric distortion. The largest filter-dependent systematics in the residuals map can be removed to a negligible level as for example seen in Figure 13.

A similar effect of the filter-dependent part of distortion was also noticed in ACS/WFC filters (Anderson 2002), where the amplitude of the filter perturbation was found to be about 0.05 pixel, spatially coherent over ∼150 pixels. It is surprising that the large amplitude of ∼0.2 pixel due to the pixel-grid irregularities was not discussed. It could be due to the fact that the early ACS/WFC distortion calibration was based just on limited number of 47 Tuc observations right after the ACS/WFC was installed on HST in 2002. Another reason could be due to the fact that the high precession of positions from the standard astrometric catalog used for calibration here revealed significant details of the ACS/WFC distortion.

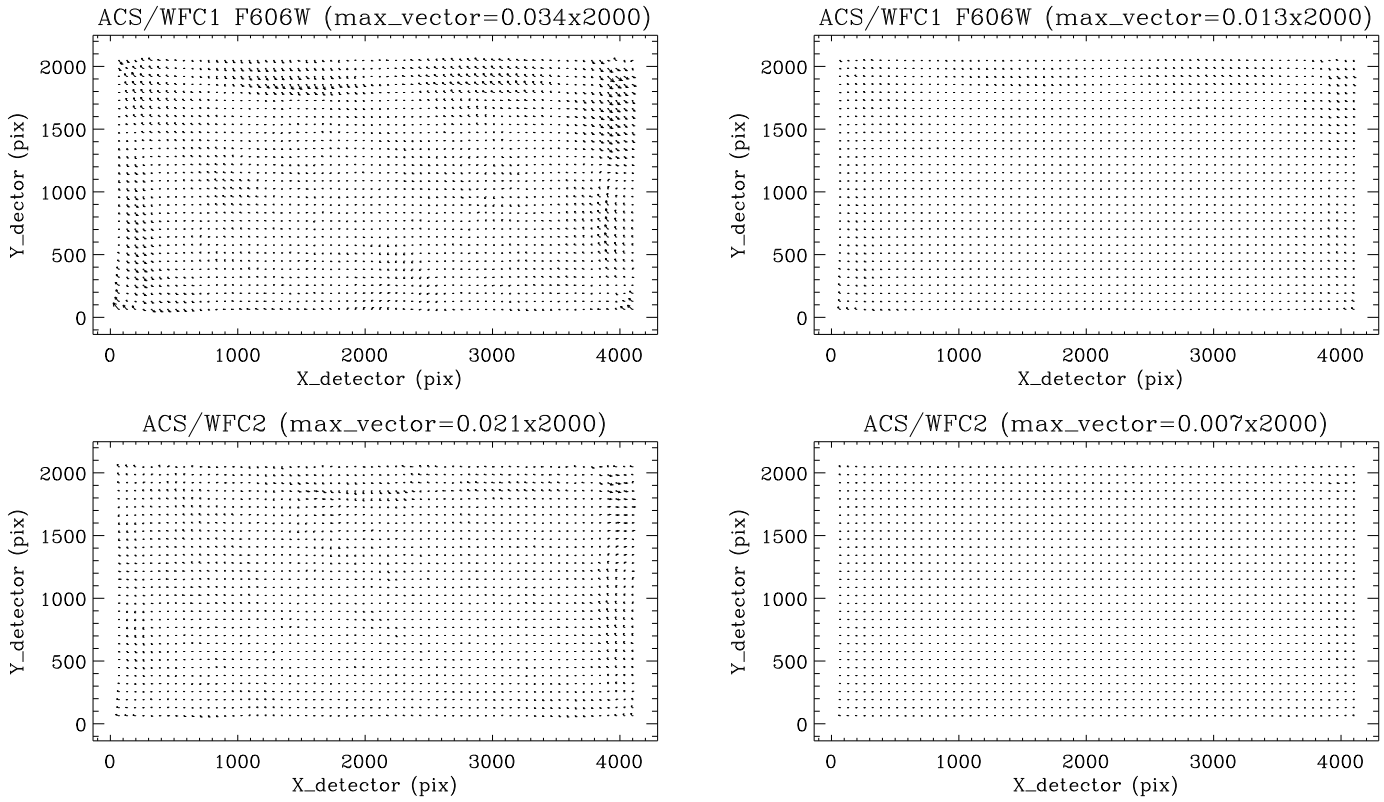

Fig. 11.— Left panel: 2-D X&Y residual map between the positions in ACS/WFC F606W filter and the standard catalog after the polynomial geometric distortion and the pixel grid irregularities are removed. The top panel shows the X&Y residuals for the ACS/WFC1 CCD chip and the bottom panel X and Y residuals for the ACS/WFC2. The largest vector is 0.032 pixel. Right panel: the same as on the left but after the correction for ACS/WFC F606W filter-dependent distortion. The largest vector is only 0.012 pixel, magnified by a factor of 2000. The units are ACS/WFC pixels.

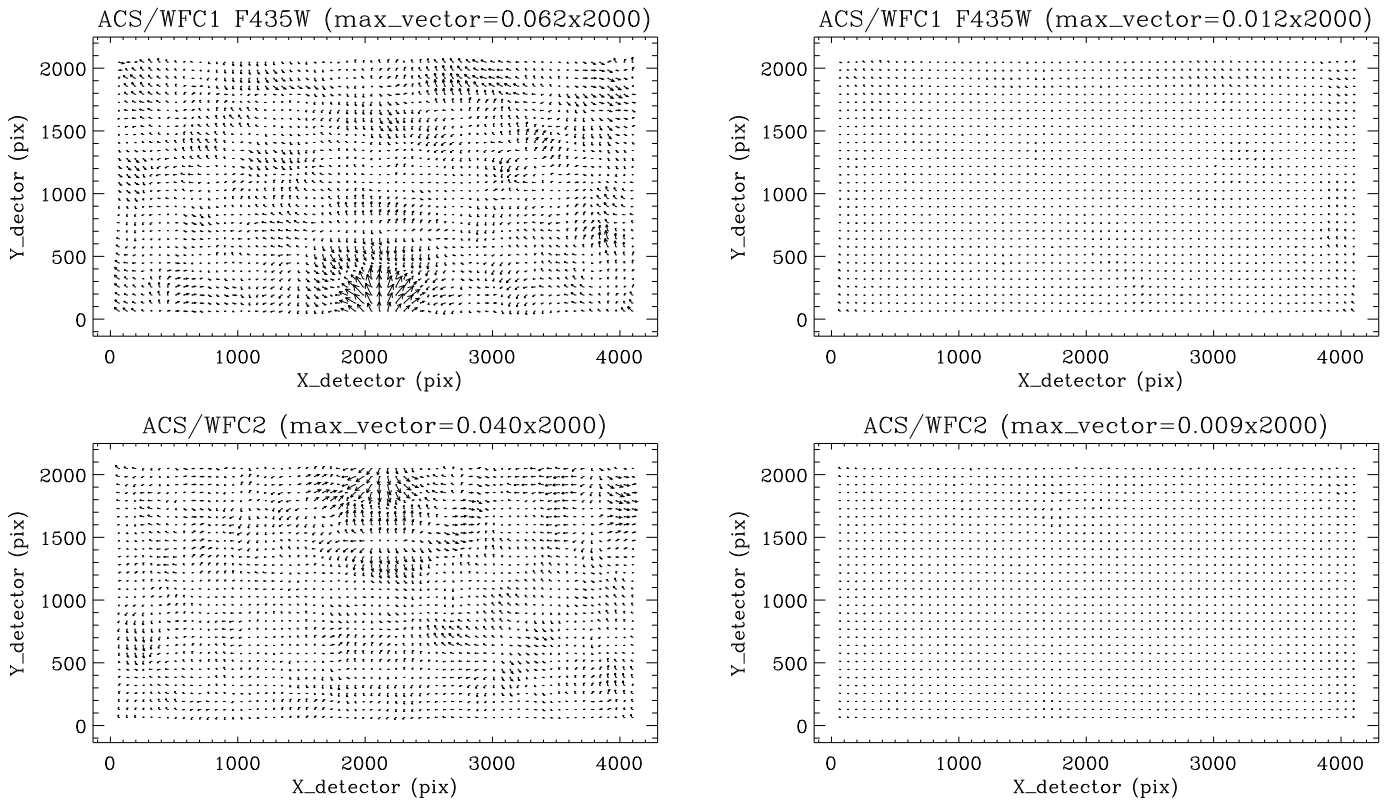

Fig. 12.— The same as Fig.11, only for the F435W ACS/WFC filter. The largest vector before correction is 0.062 pixel (on the left panel) and 0.012 pixel after correction (right panel), magnified by a factor of 2000. The units are ACS/WFC pixels.

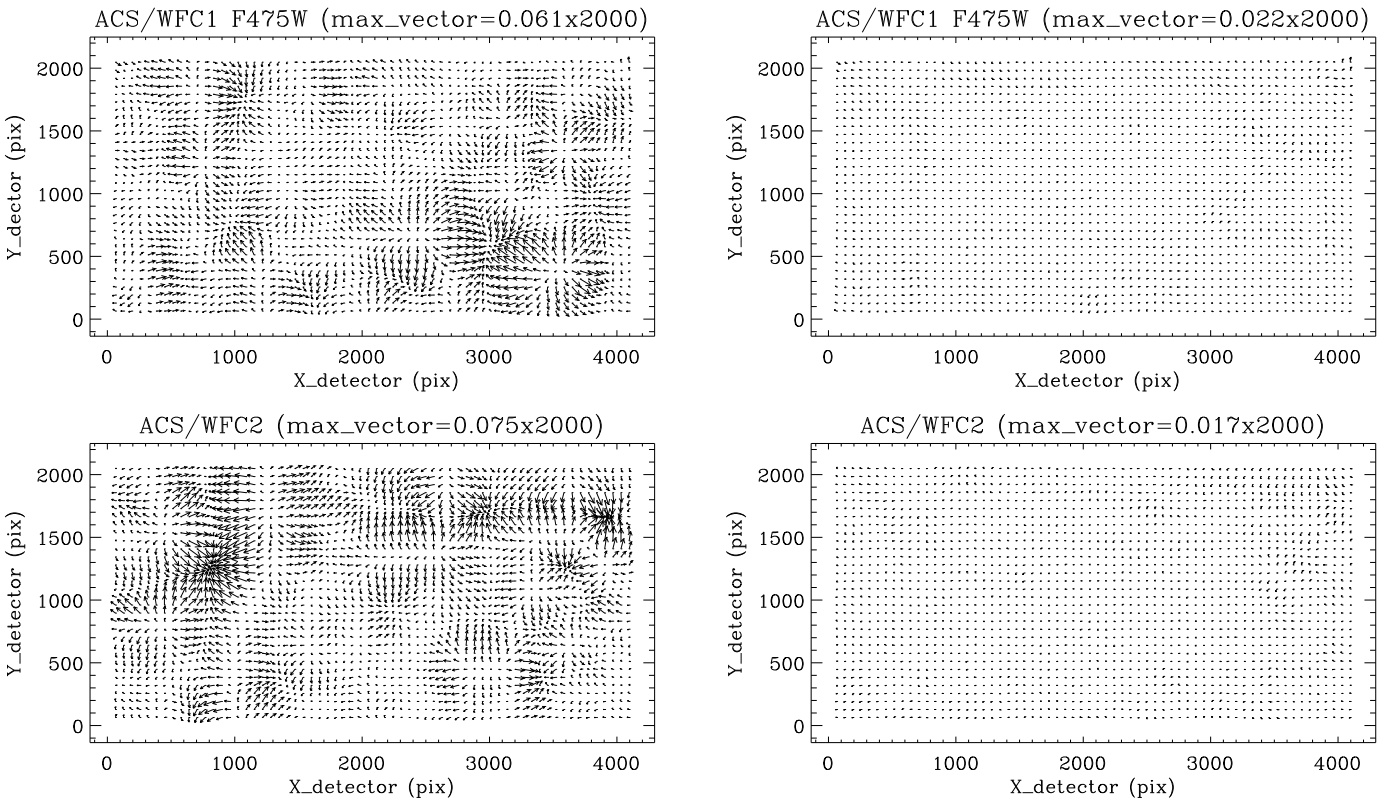

Fig. 13.— The same as Fig.11, only for the F475W ACS/WFC filter. The largest vector before correction is 0.08 pixel (left panel) and 0.02 pixel after correction (right panel), magnified by a factor of 2000. The units are ACS/WFC pixels.

4.4. Time Dependency of ACS/WFC geometric distortion coefficients

After taking out the pixel-grid irregularities using the newly- derived 2–D look-up tables and repeating the least squares minimization of the 5th-order polynomial solution, and improving it with the filter-specific distortion correction, a few iterations of the solutions allowed us to derive an accurate polynomial coefficients of geometric distortion. For each of the ACS/WFC images used for calibration and for each WFC chip, an independent solution was calculated, using the least squares minimization of the 5th-order polynomial as described in Sec.4.2. These sets of newly derived polynomial coefficients were then used to explore the noted trends in linear coefficients with time. It is a known fact that the ACS/WFC linear terms of distortion are changing with time (Anderson, 2007; van der Marel, *et al.* 2007; Ubeda, *et al.* 2013), where time dependency in linear terms are derived from the X&Y positions already corrected for geometric distortion.

Opposite to Anderson (2007) and Ubeda *et al.* (2013), a new approach for the time-dependency distortion calibration is proposed here; namely, each individual linear term out of 21 polynomial coefficients from Eqs.1–2 were investigated as a function of time. The linear terms of distortion described in Sec.4.2 are: *(i)* A_1&B_1 – the arbitrary offsets between the standard catalog and each measured frame; *(ii)* A_2&B_3 – X&Y plate–scale; *(iii)* A_3&B_2 representing the relative angle between the two X&Y axes. Thus, six linear coefficients for each ACS/WFC CCD chip from all exposures used in the solution generated a total of $2\times6\times N_{obs}$ coefficients. Some of these terms show chaotic distribution with large scatter but some of them show clear dependency with time, and some terms show a strong correlation with the HST PA_V3 roll-angle. The correlations with the HST PA_V3 roll-angle are non-linear as expected, it is rather the half-sinusoidal variation with the maximum amplitude at $\sim0^\circ$ and minimum at $\sim180^\circ$. The interpretation of such HST roll-angle dependency suggests that some linear terms have a relation to the orbit of HST, or more precisely is indicative of the velocity aberration effect. The effect of velocity aberration discussed by Cox & Gilliland (2002) is acting as the scale factor and it is measurable on ACS/WFC images. Over one HST orbit period the ACS/WFC scale can change as much as 5 parts in 100,000. Velocity aberration is a known correction factor to an image (VAFACTOR), and is available from the header of the science image. The velocity aberration factor is used in the DrizzlePac software during the geometric distortion correction through the IDCTAB. Therefore, the output from DrizzlePac as drizzled image (`*_drz.fits`) is velocity aberration free. Because of that, the polynomial coefficients from IDCTAB must be velocity aberration neutral. However, the linear terms should be also examined for how the velocity aberration may influence linear terms and how the linear terms depend on the HST PA_V3 roll-angle.

4.4.1. Constant Terms

First, we investigated the constant terms in X&Y solution, coefficients A_1 and B_1 from Eqs.1–2. The constant in X solution does not show any dependency with time, VAFACTOR or the HST PA_V3 roll angle. On the other hand, the B_1 coefficients show a large and chaotic distribution versus time for both WFC1 & WFC2 CCD chips, top and bottom left panels respectively in Fig.14. On the other hand, as seen in Fig.14 (right panel), coefficient B_1 for WFC1 CCD chip have a clear half-sinusoidal pattern as a function of the HST PA_V3 roll-angle. The maximum of B_1 for WFC1 are at $\sim$0° and $\sim$360°, which are proportional to the dot-product of the Earth motion with respect to the direction of 47 Tuc. Opposite to WFC1 constant term, coefficient B_1 for WFC2 CCD chip, there is no dependency on time or VAFACTOR and has insignificant scatter of B_1 at the level of $\pm$0.002 pixel. The keyword VAFACTOR from the header of each used image was applied to remove the expected trend for velocity aberration. Figure 15 is similar to Figure 14, but it shows the B_1 coefficients after the VAFACTOR was applied. It is clear that the scatter of B_1 coefficients for the WFC1 CCD chip as a function of time or PA_V3 angle is significantly reduced. There is some deviation of B_1 for WFC1 at the level of 0.1pix, but it is safe to adopt the mean value of Y constant in WFC1 CCD chip as $\hat{B}_1 = 2079.58\pm0.02$ pixel before SM4 and $\hat{B}_1 = 2079.53\pm0.02$ pixel after SM4. For WFC2, Y constant (B_1 coefficients) is very small, deviation from the mean of B_1 is on the level of 0.003 pixel, and averaged value of all B_1 coefficients is similar before and after SM4.

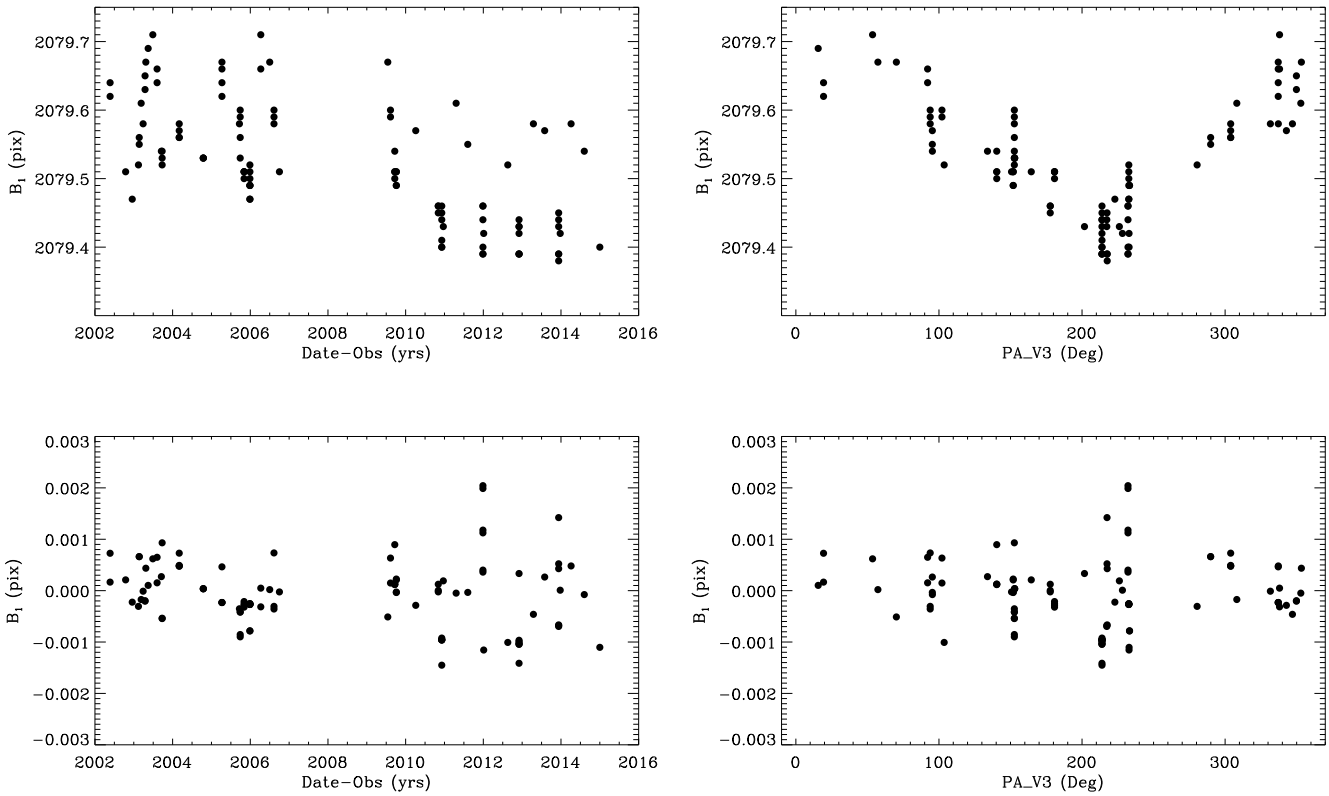

Fig. 14.— Constant term, coefficients B_1 from all sets of the polynomial solution. Top panel, from left to right: constant term for WFC1 as a function of time and the HST PA_V3 roll-angle, respectively. Bottom panel, from left to right: constant terms for WFC2 as a function of time and the HST PA_V3 roll-angle. The units are ACS/WFC pixels.

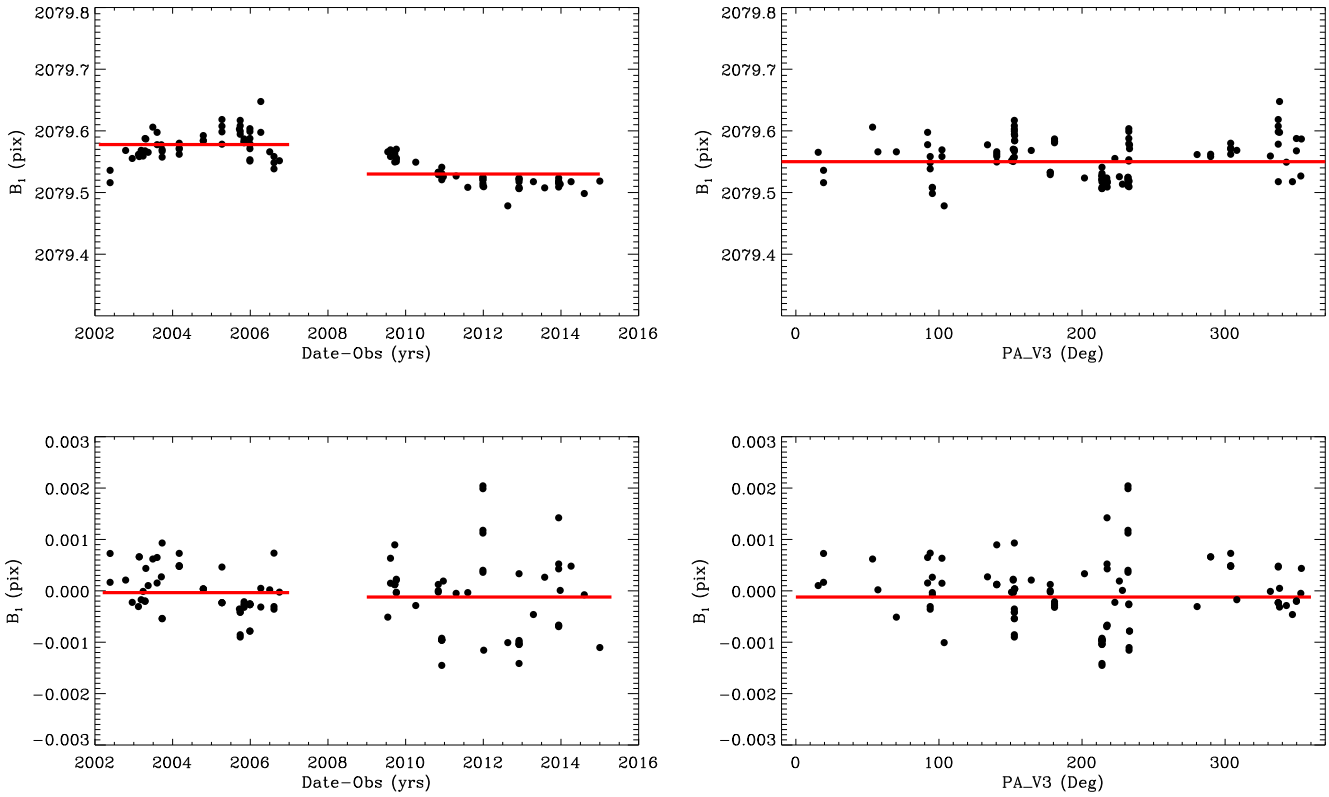

Fig. 15.— The same as Fig.14, but after the VAFACTOR was applied to B_1 coefficients. Over-plotted red lines represents the adopted mean of B_1 coefficients before and after SM4. The units are ACS/WFC pix.

4.4.2. Xscale and Yscale.

The linear terms in X and Y solutions, A_2 and B_3 coefficients from Eqs.1-2 represents *Xscale* and *Yscale*, which were also investigated as a function of time and the HST PA_V3 roll-angle.

Xscale: Figure 16 shows the A_2 coefficients as a function of time and the HST PA_V3 roll-angle. There is a noticeable linear trend with large scatter of *Xscale* as a function of time for both CCD chips. We note that *Xscale* as a function of PA_V3 roll-angle is similar to the random distribution of B_1 terms seen in Fig.14 (right panel). The maximum of *Xscale* in WFC1 and WFC2 are similar to B_1 terms from WFC1 CCD chip. As mentioned in Sec.4.4.1, the minimum and maximum of *Xscale* is proportional to the dot-product of the Earth rotation with the direction of 47 Tuc and it is related to the velocity aberration effect, as a small part of the scale factor. In order to remove this trend, the keyword VAFACTOR is applied to each A_2 coefficient. Figure 17 shows *Xscale* after applying the velocity aberration to the coefficients A_2. As seen in Figure 17, the scatter of the A_2 coefficient is significantly reduced, and provides a much tighter time-dependency of *Xscale*. However, the application of VAFACTOR has no impact on the scatter of *Xscale* as a function of PA_VA3.

A linear fit was used to find the time-dependent *Xscale* parameters:

$$X_{scale} = \alpha_{A_2} + \beta_{A_2} \times (TIME - RDATE) \tag{3}$$

where TIME is the time of observation and RDATE is defined as 2004.5 and 2012.5 before and after SM4, respectively. Parameters of this fit are given in Table 1.

Table 1: Parameters of Time-Dependency in *Xscale*

CCD	RDATE	α_{A_2}	σ_α	β_{A_2}	σ_β
WFC1	2004.5	0.98205648	9.14e-07	-9.22e-06	6.85e-07
WFC2	2004.5	0.99468101	8.65e-07	-9.16e-06	6.47e-07
WFC1	2012.5	0.98196909	1.45e-06	-2.18e-05	8.40e-07
WFC2	2012.5	0.99459657	1.36e-06	-2.26e-05	7.86e-07

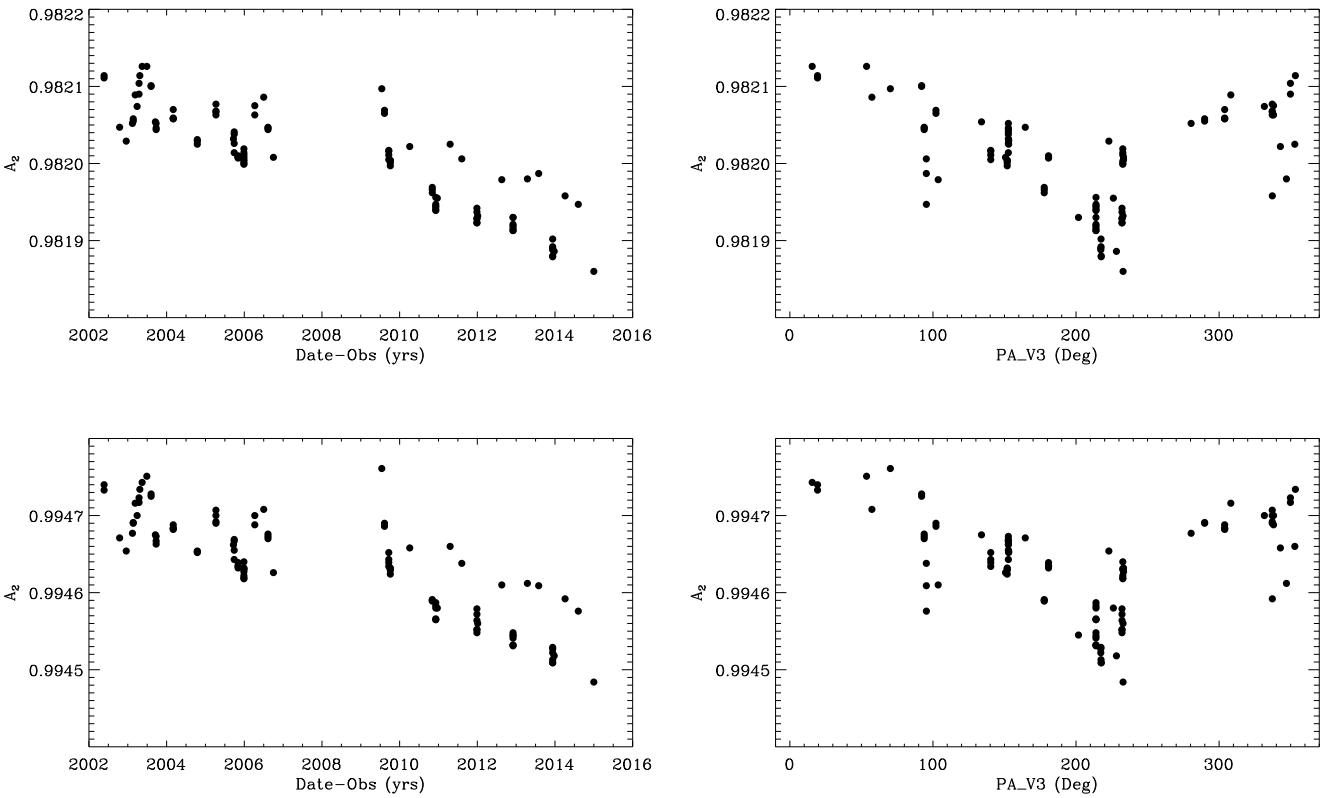

Fig. 16.— Distribution of A_2 coefficients (*Xscale*) from all sets of polynomial solution. Top panel, from left to right: *Xscale* for WFC1 as a function of time and the HST PA_V3 roll-angle. Bottom panel, from left to right: *Xscale* for WFC2 as a function of time and the HST PA_V3 roll-angle. The units are ACS/WFC pixel.

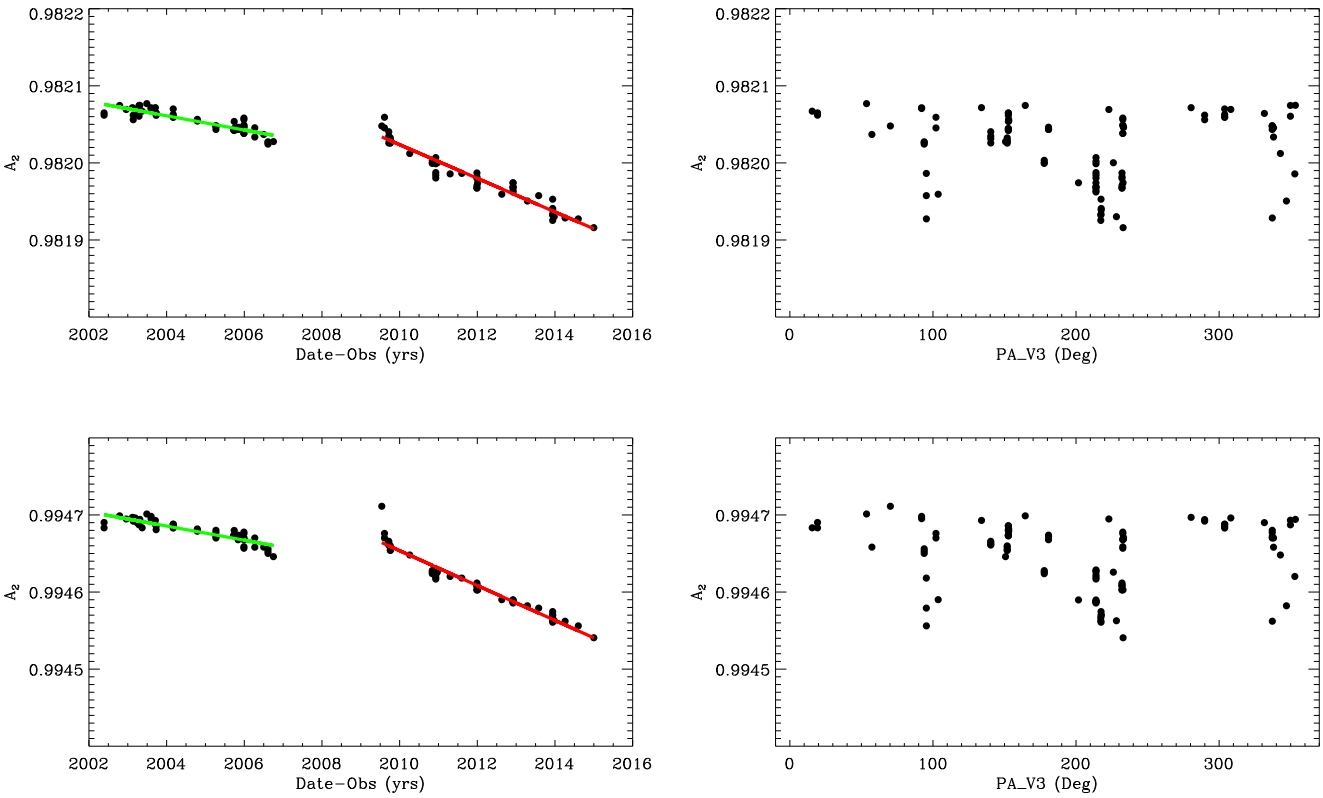

Fig. 17.— The same as Figure 16, but after the VAFACTOR was applied to A_2 coefficients (*Xscale*). Green and red lines are over-plotted linear fit before and after SM4.

After correction of *Xscale* as a function of time, seen in Fig.18, the *Xscale* is constant for both WFC CCD chips, before and after SM4. The scatter in *Xscale* as a function of PA_V3 is not only significantly reduced but it also clearly shows the *Xscale* change before and after SM4. Scaling *Xscale* by 2048 pixel (in the far edges of the CCD chips) the *Xscale* has changed by ∼20mas. It is not known yet, why the *Xscale* has changed after SM4. A similar offset in the FGS "absolute scale" has been noticed by B. McArthur (private communication), when she did the re-calibration of parallaxes with the FGS.

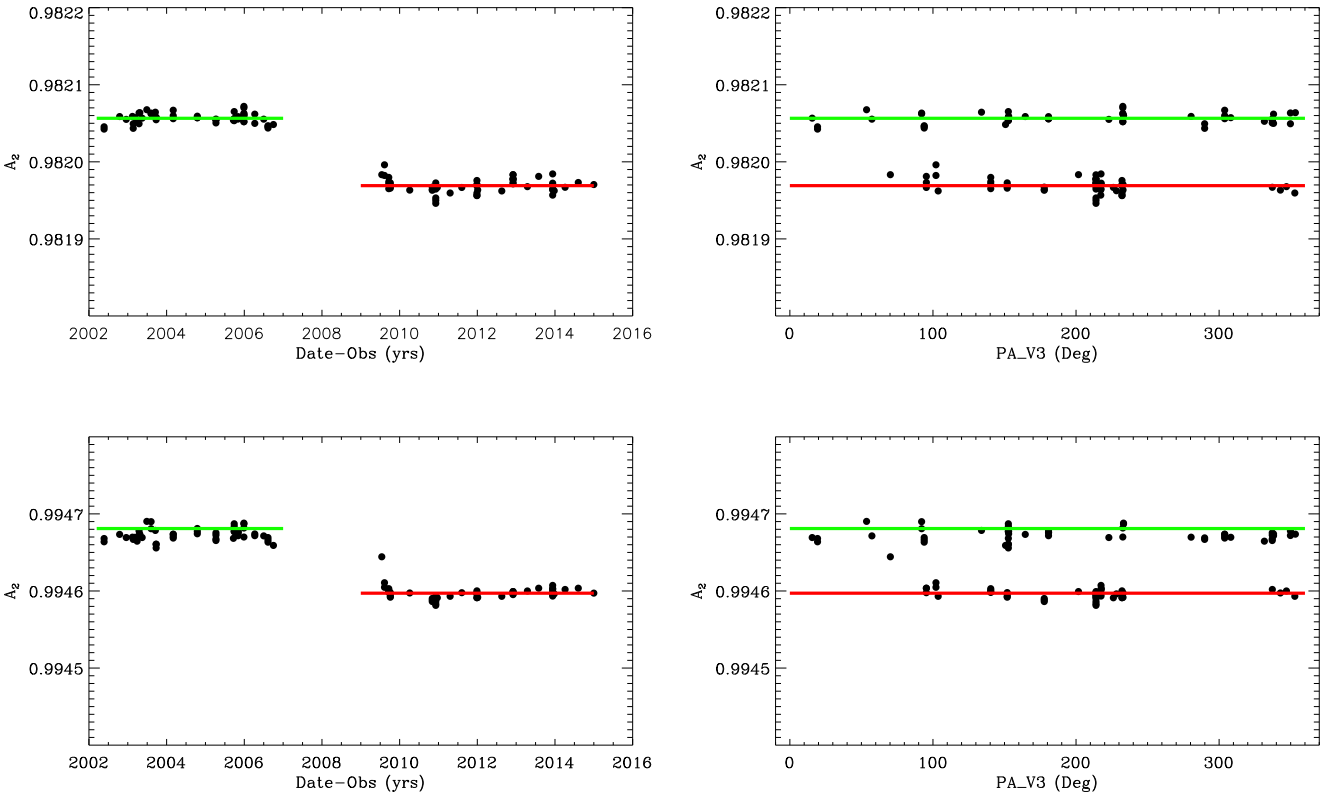

Fig. 18.— The same as Figure 17, only A_2 coefficients (*Xscale*) are now corrected for the time-dependency. Over-plotted green and red lines are the linear fit from the Eq.3.

Yscale: The linear term B_3, representing *Yscale* in all set of Eqs.2 are shown in Figure 19, as a function of time and HST PA_V3 roll-angle. The *Yscale* appears to be nearly constant with time for both CCD chips, although a large scatter is for WFC1 CCD chip. Similar to *Xscale* a maximum of *Yscale* at $\sim 0^\circ$ and $\sim 360^\circ$ is visible for WFC1 when plotted against of PA_V3, which indicates the velocity aberration effect in the scale factor.

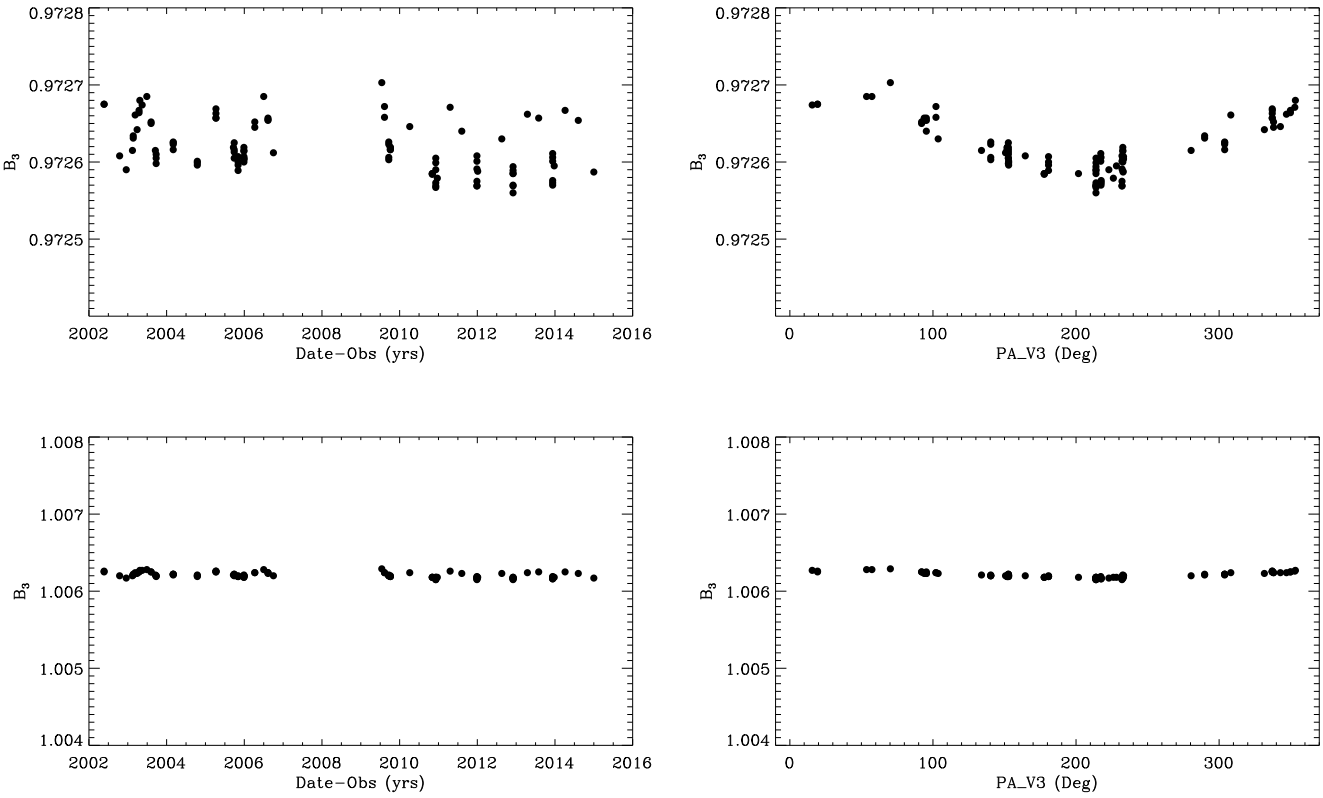

Fig. 19.— Distribution of B_3 coefficients (*Yscale*) from all sets of polynomial solutions. Top panel, from left to right: *Yscale* of WFC1 as a function of time and the HST PA_V3 roll-angle. Bottom panel, from left to right: *Yscale* of WFC2 as a function of time and the HST PA_V3 roll-angle. The units are ACS/WFC pixel.

Applying VAFACTOR to the *Yscale*, the scatter in *Yscale* for WFC1 is reduced and the *Yscale* is almost constant as a function of PA_V3 roll-angle. As seen in Figure 20, there is also very small linear trend in *Yscale* with time before SM4. Scaling *Yscale* by 1024 pixel (in the far edge of WFC1), it yields to $\sim$0.2mas/yr change in *Yscale*. Over 5 years, the difference in the *Yscale* would reach $\sim$1mas, which is insignificant for accurate alignment of the ACS/WFC images. However, the linear equation, similar to Eq.3 was used to find the

formal time-dependent parameters of *Yscale*. Parameters of the fit in *Yscale* are presented in Table 2.

Table 2: Parameters of Time-Dependency in *Yscale*

CCD	RDATE	α_{B_3}	σ_α	β_{B_3}	σ_β
WFC1	2004.5	0.97263238	1.25e-06	2.42e-06	9.37e-07
WFC2	2004.5	1.00622300	1.29e-06	3.30e-06	9.65e-07
WFC1	2012.5	0.97263233	1.41e-06	-1.12e-06	8.17e-07
WFC2	2012.5	1.00621870	1.13e-06	-8.04e-07	6.52e-07

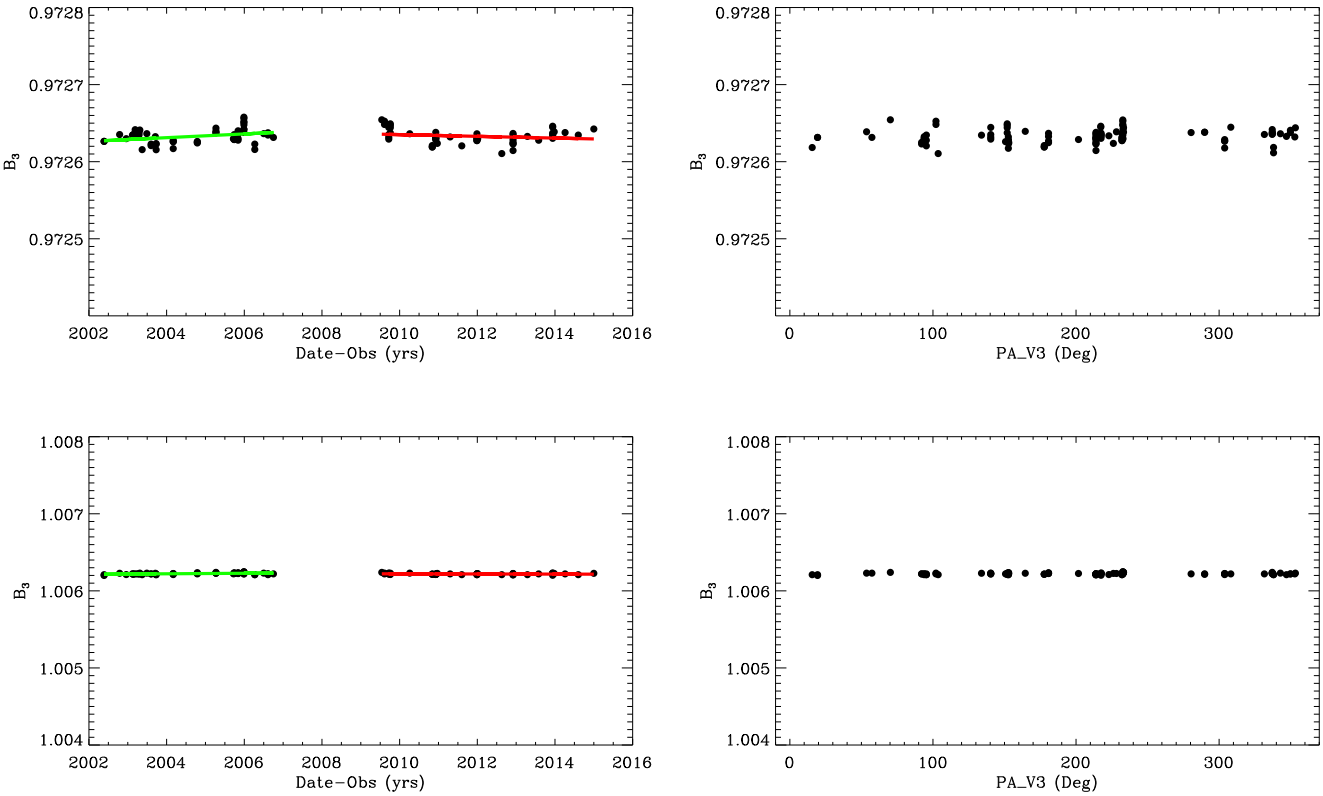

Fig. 20.— The same as Figure 19, but for B_3 coefficients (*Yscale*) after VAFACTOR was applied. The green and red lines are linear fits of *Yscale* as function of time, before and after SM4.

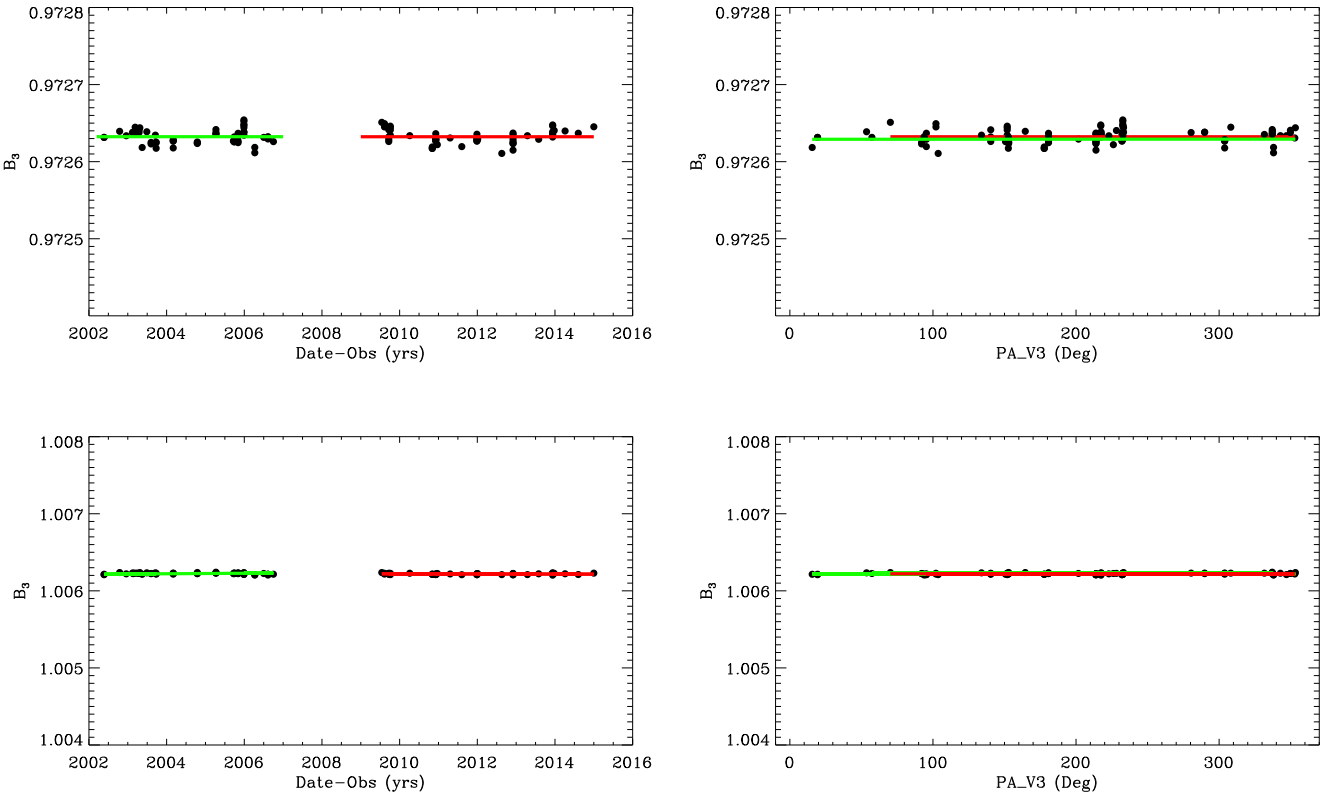

Fig. 21.— The same as Figure 20, but B_3 coefficients (*Yscale*) are corrected for the time-dependency. The green and red lines are linear fits of *Yscale* as function of time, before and after SM4.

After correction of *Yscale* in WFC1, it is clear that there is no offset in *Yscale* before and after SM4 which is observing in *Xscale*. It is interesting to note that *Yscale* is essentially constant in WFC2. The reason why the ACS/WFC scale has changed after SM4 only in one axis is not clear and not understood yet. The scope of this work is only to look for possible variations of distortion coefficients, and if found, to provide an accurate and stable solution for the ACS/WFC geometric distortion.

4.4.3. Residual Rotation in X&Y.

Two linear coefficients in Eqs.1-2, A_3 and B_2 are indicative of rotation between the two coordinates systems, the standard astrometric catalog (U&V) and the measured frame (X&Y). Significant ACS/WFC linear distortion, known as the skew terms, which are characteristic of the amount of non-orthogonality between the two principal axes. The deviation from non-orthogonality in X-axis & Y-axis is θ angle which is off by a small amount from the nominal 90° angle between two axes. As described in Sec. 4.2, WFC2 was chosen as basic reference frame for the meta-chip solution and its X-axis used as a primary reference axis, by minimizing the ratio of linear terms A_3/B_2. Because of that, the amount of deviation from non-orthogonality in X-axis is almost zero in WFC2 CCD chip (*i.e.* ±2e-10). The deviation of the angle θ in X-axes for WFC1 however is large, because it includes the gap between two CCD chips and the rotation angle between the CCD chips at the central point of each chip. The θ angle in X-axis for WFC1 is also constant with time.

Contrary to the A_3 coefficients, the angle θ in Y axis (B_2 coefficients) for both CCD chips is not only large but also significantly changing with time. As expected there is no influence of the velocity aberration and PA_V3 roll-angle on A_3 & B_2 since the velocity aberration affect only the scale (Cox & Gilliland, 2002). The evolution of B_2 is similar to A_2 in Figure 17 only in opposite directions: A_2 (*Xscale*) has contracted with time, B_2 has expanded with time. These two opposite directions of A_2 and B_2 correspond to the linear shear of two significant geometric distortion terms. As seen in Figure 22, B_2 changes by ∼2mas/yr in WFC1 and in WFC2, when scaled by 1024 pixel at the far edges of WFC1 and WFC2. This large amount of skew is detrimental for accurate alignment of ACS/WFC images, particularly if the images are taken over a large span of time.

Similar to the *Xscale* and the *Yscale* (Eq.3, Sec.4.4.2), a linear fit was used to find the parameters of B_2 time-dependency. Parameters of fit of B_2 are presented in Table 3.

Table 3: Parameters of Time-Dependency in *Residual rotation*

CCD	RDATE	α_{B_2}	σ_α	β_{B_2}	σ_β
WFC1	2004.5	0.080947069	9.206e-07	3.617e-05	6.893e-07
WFC2	2004.5	0.068598586	9.211e-07	3.532e-05	6.897e-07
WFC1	2012.5	0.081139194	2.450e-06	3.235e-05	1.418e-06
WFC2	2012.5	0.068779336	2.255e-06	3.070e-05	1.305e-06

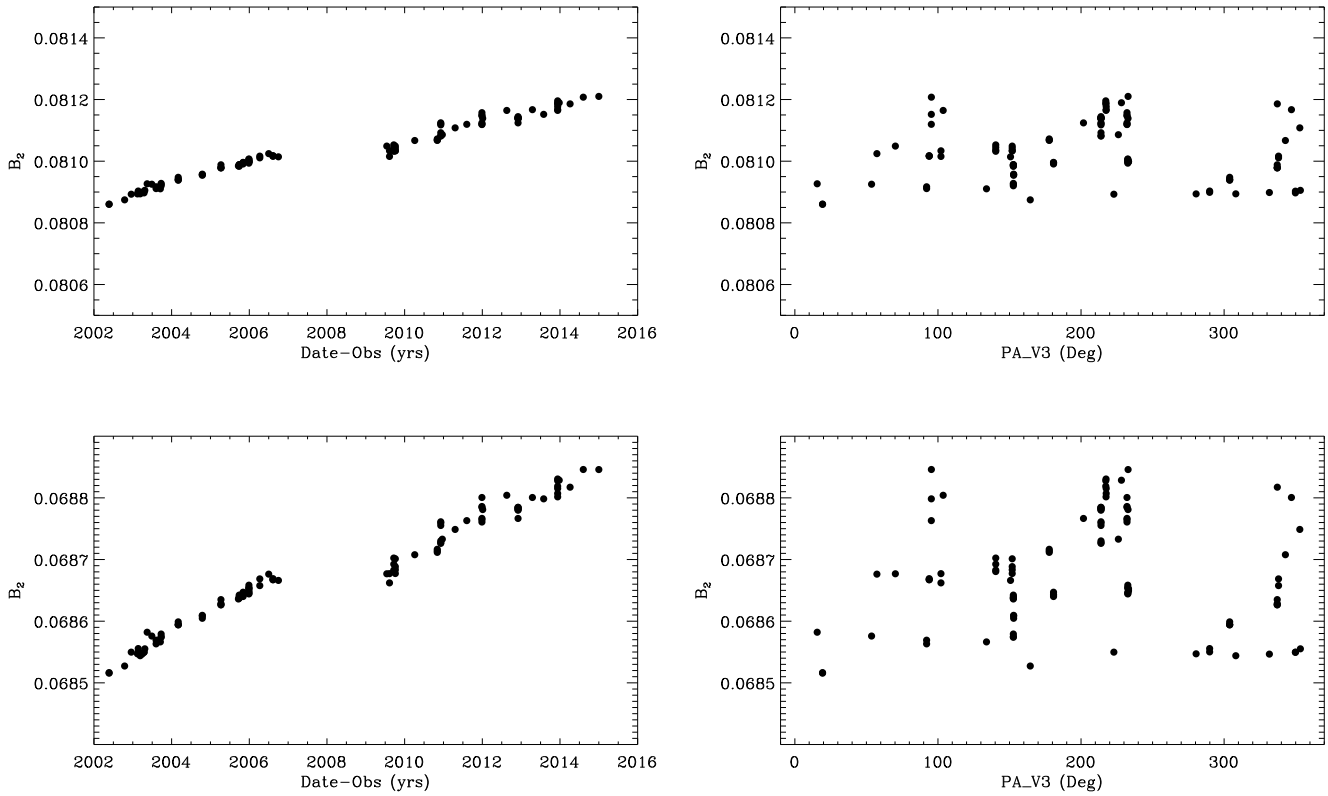

Fig. 22.— Distribution of the the B_2 coefficients, the residual rotation in Y solutions, from all sets of the polynomial solution. Top panel, from left to right: B_2 coefficients for WFC1 as a function of time and the HST PA_V3 roll-angle. Bottom panel, from left to right: B_2 coefficients for WFC2 as a function of time and the HST PA_V3 roll-angle. The units are ACS/WFC pixel.

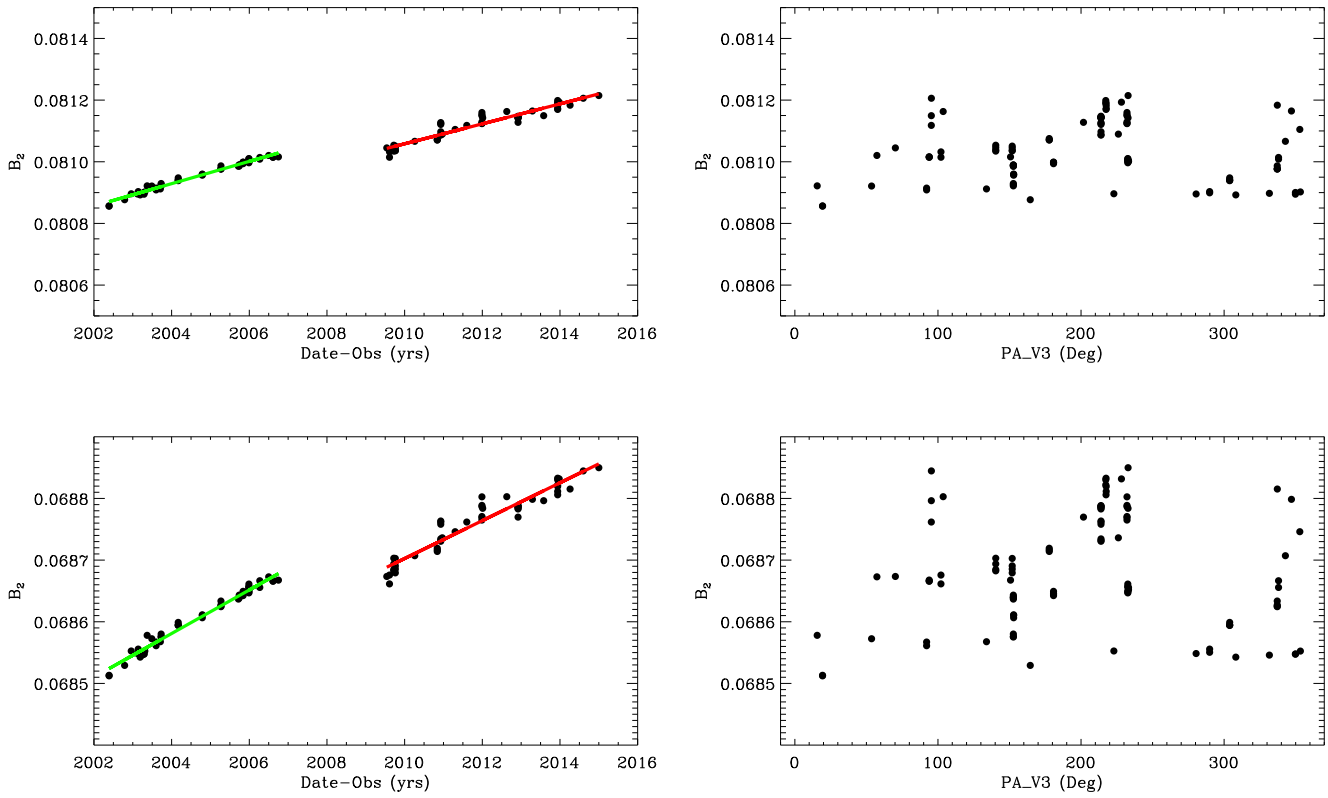

Fig. 23.— The same as Figure 22, only for B_2 coefficients after VAFACTOR was applied. Over-plotted red and green lines represent a linear fit.

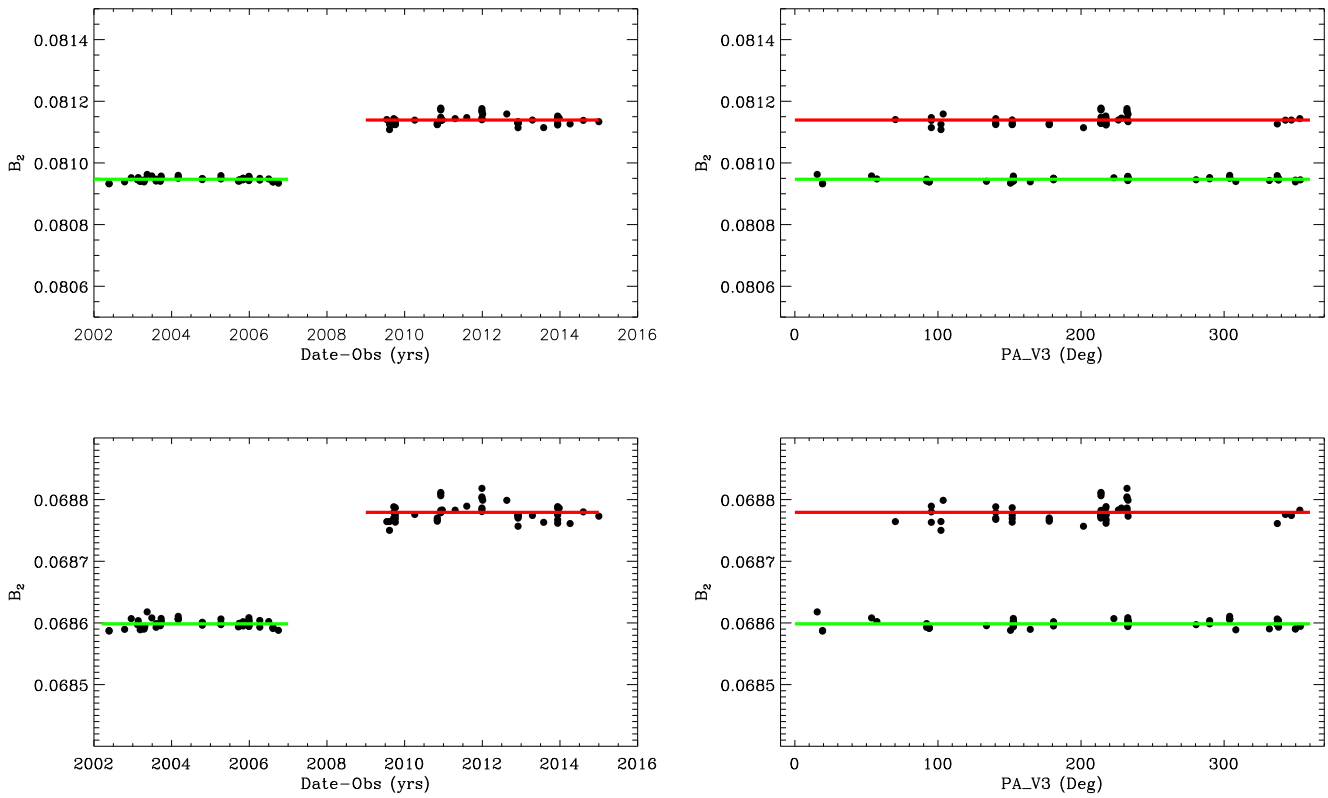

Fig. 24.— The same as Figure 23, but B_2 are now corrected for time-dependency.

Applying the parameters of a linear fit from Table3, the scatter in B_2 is significantly reduced, and the distribution of coefficients B_2 is constant (Figure 24, left panel). The scatter of B_2 is also reduced in the plot showing B_2 as a function of PA_V3. Similar to *Xscale* two populations of the B_2 coefficients are visible. The offset between in B_2 before and after SM4 is ∼9.3mas for WFC1 and ∼9.8mas for WFC2 scaled by 1024.0 at the far edges for both CCD chips. The offset in B_2 before and after SM4 is similar to the offset in A_2 terms as seen in Figure 18. These two terms have changed during SM4 for unknown reasons, as discussed in Sec.4.4.2.

4.4.4. Time-Dependency Correction is Filter-Independent

The newly obtained linear parameters β_{A_2} and β_{B_2} of time-dependency in A_2 and B_2 terms (see Table 2,3) should be used to correct these terms in Eq.1-2 (Sec.4.2) as follows:

$$\grave{A}_2 = A_2 - \beta_{A_2} \times (TIME - RDATE) \tag{4}$$
$$\grave{B}_2 = B_2 - \beta_{B_2} \times (TIME - RDATE) \tag{5}$$

where A_2, B_2 are the coefficients from Eqs.1–2, averaged from all sets of polynomial solution; and the argument TIME and RDATE as above in Eq.3. Thus, the linear coefficients in Eqs.1–2 must be replaced by updated coefficients $\grave{A}_2$ and $\grave{B}_2$ from Eqs.4–5 to correct $X\&Y$ raw positions from ACS/WFC images for the geometric distortion and simultaneously correct for its time-dependency.

The linear parameters of the time-dependent distortion were derived using the observations through the F606W filter only. Each filter has its own fine-scale solution as discussed in Sec.4.3.2 and should have also a different plate-scale. Variation of the scale with a filter is due to the thickness of filter itself. The image-scale is strongly correlated with the central wavelength of the filter. In the case of WFC3/UVIS, the relative scale changes from filter to filter by ∼0.02% (Kozhurina-Platais *et al.*, 2012). As discussed by Anderson (2002), the scale for different ACS/WFC filters do not possess much difference, except for F814W. Does the time-dependent distortion change from filter to filter?

In order to show that the time-dependency does not change with filter, coefficients A_2 and B_2 from Eq.1-2 are plotted as a function of time similar to Figure 17 and Figure 23 shown F606W, but now for three other filters, F435W, F475W, F814W. Figure 25 shows corrected A_2 terms for time-dependency as a function of time. As seen in Figure 25, applying the linear parameters of time-dependency to A_2, it is constant for all four calibrated filters

and for over entire lifetime of ACS/WFC. It is also clear that the plate-scale (*Xscale*) is different from filter to filter. According to Figure 25, *Xscale* for F435W and F475W is almost identical, but differs from F606W by ∼0.05 pix and ∼0.2 pix from F814W. On the other hand, the scale difference between in F606W and F814W is at the level of ∼0.1 pix. The offset in *Xscale* before and after SM4 for all three ACS/WFC filters does not change.

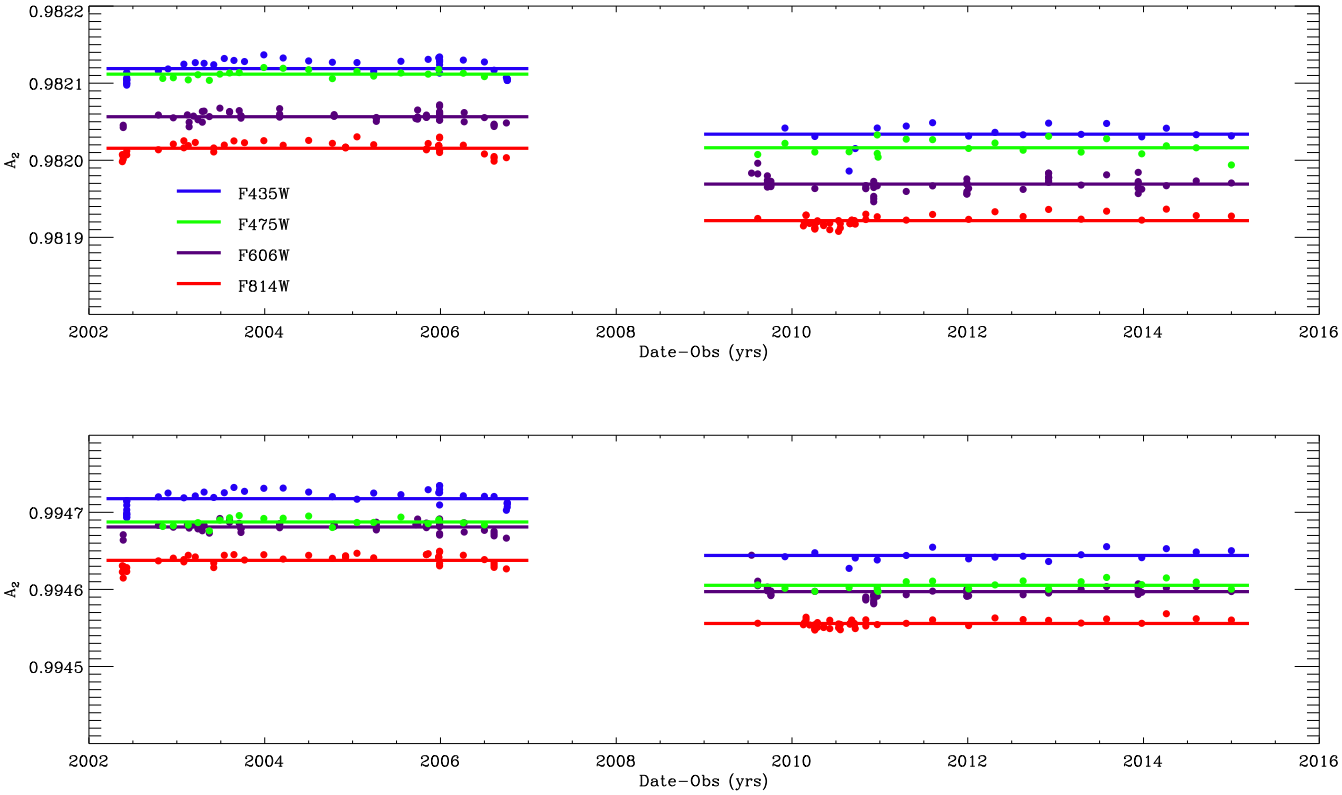

Fig. 25.— Distribution of A_2 coefficients (*Xscale*) for the selected ACS/WFC filters. The blue, green, violet and red lines are *Xscale* for F435W, F475W, F606W and F814W ACS/WFC filters after correction for time-dependency. From top to bottom: A_2 coefficients for WFC1 and WFC2, respectively.

As seen in Figure 26, the B_2 coefficients from four filters are almost identical except for F814W in WFC2 CCD. The difference between the B_2 coefficients in F814W and for the other three - F606W, F435W and F475W, is at the level of ∼0.06pix over WFC2 FOV. Thus, accounting for the offset of different filters in coefficients A_2 and B_2 of the geometric distortion model and accounting for non-polynomial component of filter distortion (shown in Sec.4.3.2) are important for various ACS/WFC and HST cross-instruments programs to combine and align HST images taken in different filters.

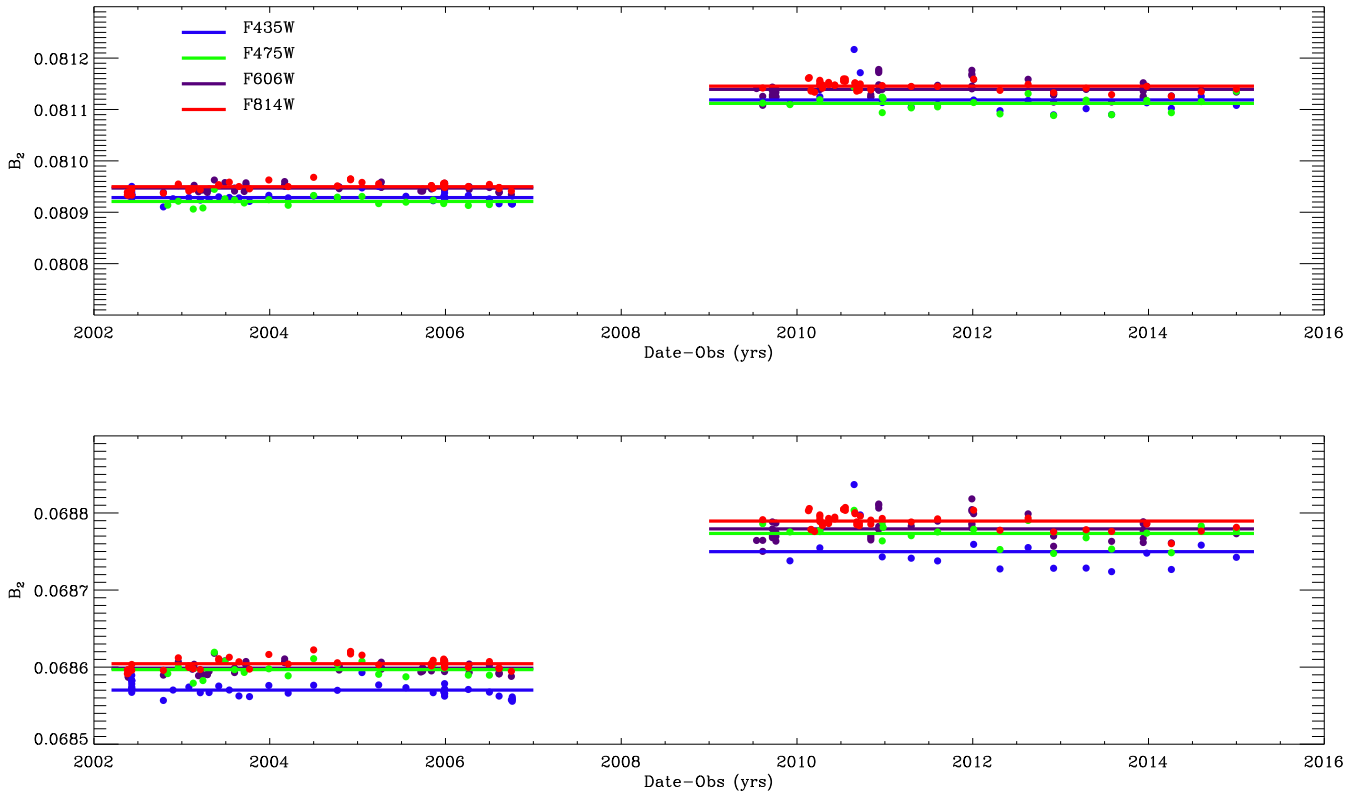

Fig. 26.— The same as Figure 25, only for B_2 coefficients after time-dependency correction for the four ACS/WFC filters.

5. Instrument Distortion Coefficients Table - IDCTAB

The newly-derived coefficients of geometric distortion for the ACS/WFC channel are in the system of X and Y detector coordinates, which can be used to correct the X and Y positions obtained from any ACS/WFC `(*_flt.fits)` image with arbitrary pointing and orientation. The geometric distortion coefficients are fundamental for on-the-fly calibration in the STScI (OTFR) pipe-line in order to remove the distortion from these ACS/WFC images, which are called drizzled `(*_drz.fits)` images. These coefficients are stored in a reference file – Instrument Distortion Coefficients Table (IDCTAB), which, however, is in the HST-based coordinates system – V2&V3. A detailed description of the IDCTAB reference file can be found in Hack & Cox (2001). Thus, the geometric distortion coefficients in the X&Y detector coordinate system must be converted into the V2&V3 system (equivalent to the sky tangential plane) including the scaling and distortion correction with the origin at the reference position where the detector and the sky axes are exactly parallel. A full description of the V2&V3 system and the transformation of the X&Y detector coordinate system into the V2&V3 system is provided by Borncamp *et al.* (2014). There is also provided a full description how to transform polynomial coefficients (Eqs.1–2) into the IDCTAB format.

In the current ACS/WFC IDCTAB the linear parameters of the time-dependent distortion (TDD) are based on the original Anderson (2007) correction, which is in the X&Y detector coordinate system. Since the IDCTAB is in the of HST V2&V3 coordinate system, therefore the TDD correction has to be converted into the V2&V3 system. It is not trivial to transform the linear parameters of the TDD fit from one coordinates system into another, it is a complicated numerical manipulation which may introduced model-dependent systematic. Nevertheless such a transformation was performed by the following steps: (1) each linear coefficient for each CCD chip from IDCTAB formalism was converted (i.e. shifting and rotating) back to the X&Y detector coordinates system; (2) then each linear term for each CCD chip was corrected for the linear TDD; (3) the corrected linear coefficients were shifted and rotated back into IDCTAB formalism. Although the original TDD correction is applied to X&Y, corrected for distortion as single frame, the same values of TDD correction were applied to the linear terms of WFC1 and as to the linear terms of WFC2. Such complicated numerical manipulation of the linear terms in IDCTAB resulted in a poor alignment ($\sim$0.2 pix) of ACS/WFC images.

To avoid the complicated numerical manipulation of IDCTAB, we offer a straightforward way to implement TDD in IDCTAB. Here, we outline only the principal steps pertaining to the time-dependency of the linear terms:

- each set of polynomial coefficients (Eqs.1–2) from each individual solution were indi-

vidually transformed into the IDCTAB, resulting in a total of N_{obs} IDCTAB;

- VAFACTOR from the header of each observation used for the geometric distortion solution was applied to the coefficients from each IDCTAB to to remove the expected trend for velocity aberration for each coefficient in each IDCTAB;
- similar to (Eq.3), linear parameters of time-dependency in linear terms from each IDCTAB were derived, so that parameters of the time time-dependency are also now in the V2&V3 system;
- coefficients from each IDCTAB were then averaged so that the mean coefficient from all sets of the IDCTABs now form a single IDCTAB.

Thus, the time-dependent distortion instead of IDCTAB manipulation is now hard coded in the new STDAS software DrizzlePac in the straightforward way, similar to Eqs.4–5, as follows:

$$C\grave{X}11 = CX11 - \beta_{CX11} \times (TIME - RDATE) \quad (6)$$
$$C\grave{Y}10 = CY10 - \beta_{CY10} \times (TIME - RDATE) \quad (7)$$

where CX11 and CY10 are averaged linear coefficients in IDCTAB formalism and correspond to A_2 and B_2 in Eqs.1–2 for each CCD chip, WFC1 and WFC2, and for each individual ACS/WFC filter.

Parameters of the linear time-dependency β_{CX11}, β_{CY10} and $RDATE$ (2004.5 and 2012.0 before and after SM4) are kept in the primary header of the IDCTAB. Since the plate-scale and the parameters of the linear time–dependent distortion are slightly different before and after SM4, two IDCTAB (before and after SM4) are provided to the user and to the HST-data-base reference system to be used in DrizzlePac and the HST pipe-line.

6. Test with the DrizzlePac/TweakReg

The new software *DrizzlePac* (Gonzaga, *et al.*, 2012) developed recently by STScI has replaced the old *MultiDrizzle* software. The *DrizzlePac* software is designed to align and combine the HST images. In *DrizzlePac* there are a few tasks that can be used to perform astrometric transformations between the HST images such as a shift, rotation and scale in order to find preliminary astrometric input for *Astrodrizzle* to align and combine HST images. One such task is *TweakReg*, an automated interface that computes the offset, scale and rotation between HST images. This task uses `*_flt.fits` files as input, finds X and Y positions in these images (similar to IRAF/DAOFIND), corrects X and Y positions for geometric distortion using the reference files (D2IMFILE, NPOLFILE & IDCTAB), and solves for a shift, scale and rotation between the input images (similar to IRAF task XYXYMATCH).

Thus, to test newly-derived geometric distortions reference files, such as IDCTAB, D2IMFILE and NPOLFILE and parameters of the time-dependent distortion (TDD), we used two ACS/WFC images with observations of Large Magellanic Cloud, listed in Table 4.

Table 4: ACS/WFC Observations of Large Magellanic Cloud

Proposal ID	Date yy-mm-dd	α (°)	δ (°)	POSTARG1 (″)	POSTARG2 (″)	PA_V3 (°)	Exp Sec
10753	2006-04-25	80.49021	-69.49836	−3.75	2.5	136.97	343.0
10753	2006-07-11	80.49021	-69.49836	45.00	−45.00	−148.03	423.0

Figure 27 show the residuals of X and Y positions between these two images from the output of DrizzlePac/TweakReg (using a custom–made plotting routine). The pattern of the residuals (the left panel of Fig.27) with the current reference files in OPUS exhibit patchy areas with opposite directions of the vector flow. This pattern is due to the inaccurate correction for geometric distortion and its time dependency. The right panel of Fig.27 shows that once the newly–derived reference files, D2IMFILE, IDCTAB, NPOLFILE and new TDD parameters are applied, the complicated patchy pattern of residuals is gone. It is smooth across the entire overlapping area between two ACS/WFC images. The amplitude of residuals is reduced down to ∼0.08 pixel. Therefore, we conclude that with newly-derived distortions and TDD parameters significant improvement has been achieved.

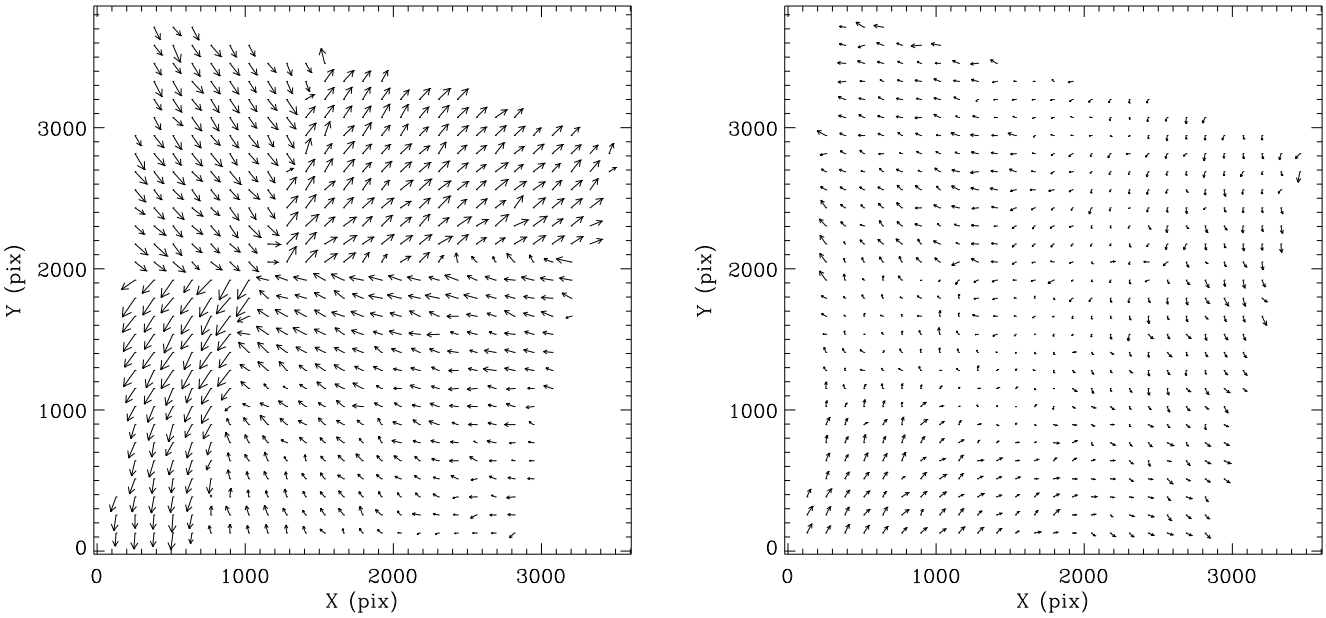

Fig. 27.— 2-D X and Y residual map between two ACS/WFC images from Table4. Left panel shows the residuals obtained with the current reference files in OPUS while the right panel shows the residual map after applying the new improved reference files. The largest vector with old reference files is ∼0.2 pixel but ∼0.08 pixel after the correction with new, both magnified by factor of 1000. The units are ACS/WFC drizzle pixels.

Nevertheless, there is still some flow of the vectors increasing towards the edges (the right panel of Fig.27), which is indication of the un-accounted skew-related linear terms in the distortion solution. The geometric skew still visible in Figure 27 (right panel) most likely is the pixel-phase errors in the measurement of undersampled PSF (Anderson & King, 2000). Inaccuracies in the measurement of X and Y positions from undersampled images induce the systematic bias in the measured positions. Therefore, the X and Y positions from both images were obtained with ePSF as described in Sec.3. These positions were used then as input in TweakReg. Figure 28 shows the residuals of X&Y positions obtained with ePSF fitting positions.

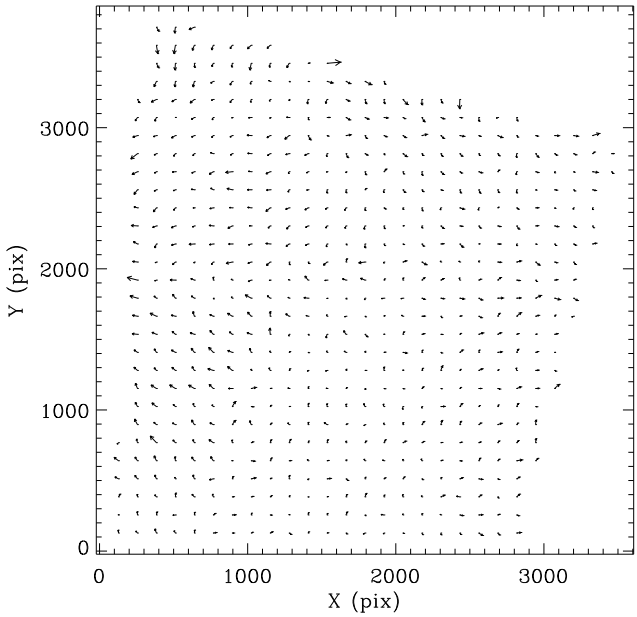

Fig. 28.— The same as Figure 27, but now the X and Y positions are derived with ePSF fitting and processed through TweakReg. The largest vector now is only ∼0.02 pixel compared to the largest vector in Figure 27. The units are ACS/WFC drizzle pixels.

The vector residual map shows significant improvement in the the vector flow, it is smooth across of the entire overlapped area between two ACS/WFC images and the largest vector is 4 times smaller than using the simple centering routine in TweakReg.

Thus, the precision of X&Y positional measurements of undersampled ACS/WFC images will directly impact astrometry and the ultimate accuracy of the geometric distortion.

7. Conclusions

This report presents a detailed description of the results of the geometric distortion calibration for the *ACS/WFC* channel. The well-planned observations of 47 Tuc in various dither patterns over entire life of ASC/WFC in combination with the techniques of an astrometric standard fields allow us to characterize the *ACS/WFC* geometric distortion down to the 2 *mas* precision level, which is four times better than the required precision.

Summarizing the newly-derived results of the geometric distortion solution for *ACS/WFC*, we conclude that besides the optical geometric distortion, there are a strong short-scale dis-

tortions coming from irregularities in the pixel grid of the ACS/WFC detector itself and in the various ACS/WFC filters used for calibrations. The irregularities in the pixel grid appear to be embedded into the supposedly regular grid of pixels during the manufacturing process of the CCDs. The amplitude of these irregularities in the pixel grid can reach in amplitude up to about 0.4 pixels (equivalent to 20mas) and varies across the ACS/WFC detector. On top of these irregularities, the expansion of the X and Y linear terms in geometric distortion with time were found. The changes in the X and Y linear terms with time are small and less than a few milli-arc-seconds per year on the sky, but large enough to introduce geometric skew in ACS/WFC images. The derived geometric distortion coefficients in the form of the IDCTAB and new representation of time-dependent distortion has already successfully been used in STSDAS/DrizzlePac software for: (1) stacking of *ACS/WFC* images with different dither pattern; (2) rejecting the CRs; (3) enhancing the spatial resolution; (4) deepening the detection limit.

8. Acknowledgments

We express our gratitude to Dan Coe for reviewing this ISR and for his useful comments and suggestions which improved significantly the clarity of ISR. We thank David Golimovski & Marco Siriani for lengthy discussion the pixel-grid irregularities in ACS/WFC manufacturing process. V.K.-P. is grateful to B. MacArthur for useful discussion of the ACS/WFC absolute scale changed after SM4.

References

Anderson, J., King, I., 1999, PASP, 111, 1095

Anderson, J., King, I., 2000, PASP, 112, 1360

Anderson, J., King, I., 2003, PASP, 115, 113

Anderson, J., 2002, in "2002 HST Calibration Workshop", eds. A.Arribas, A. Koekemoer, B.C. Whitmore (Baltimore:STScI), p.18

Anderson, J., 2005, in "2005 HST Calibration Workshop", eds A. Koekemoer, P. Goudfrooij, L. Dressel (Baltimore:STScI), p.11

Anderson, J., & King, I., 2006, ACS Instrument Science Report, ACS-ISR - 2006–01(Baltimore:STScI)

Anderson, J., 2007, ACS Instrument Science Report, ACS-ISR - 2007–08 (Baltimore:STScI)

Anderson, J., Bedin, L., 2010, PASP, 122, 1035

Bedin, L., Smith, L., 2013, ACS-ISR (not published)

Bellini, A., Anderson, J., Bedin, L., 2011, PASP, 123, 622

Borncamp, D., Kozhurina-Platais, V., Cox, C., 2014, ACS Technical Instrument Report, ACS-TIR-2014–02 (Baltimore:STScI)

Cox, C., Gilliland, R., 2002, in "'2002 HST Calibration Workshop", eds. A.Arribas, A. Koekemoer, B.C. Whitmore (Baltimore:STScI), p.58

Golimowski, D., & Sirianni, M., 2014, (private communication)

Gonzaga, S., *et al.*, 2012, "The DrizzlePac Handbook", (Baltimore:STScI)

Hack, W., Cox, C., 2001, ACS Instrument Science Report, ACS-ISR - 2001–08(Baltimore:STScI)

Koekemoer, A.,M., Fruchter, A., Hook, R.,N., Hack, W., 2002, in "2002 HST Calibration Workshop", eds A.Arribas, A. Koekemoer, B.C, Whitmore (Baltimore:STScI), p.337

Kozhurina-Platais,V., Biretta, J., 2004, ACS Instrument Science Report, ACS/ISR - 04–10 (Baltimore:STScI)

Kozhurina-Platais,V., Goudfrooij, P., Puzia, T. H., 2007, ACS Instrument Science Report,ACS/ISR-2007-04,(Baltimore:STScI)

Kozhurina-Platais, V., Cox, C., McLean, B., Petro, L., Dressel, L., Bushouse, H., Sabbi, E., 2009a, WFC3 Instrument Science Report, WFC3-ISR-2009-33,(Baltimore:STScI)

Kozhurina-Platais, V., Cox, C., McLean, B., Petro, L., Dressel, L., Bushouse, H., 2009b, WFC3 Instrument Science Report, WFC3-ISR-2009-34,(Baltimore:STScI)

Kozhurina-Platais, V., *at al.*, 2010, in "2010 HST Calibration Workshop", eds Deusta, S., Oliveira, C., (Baltimore:STScI)

Kozhurina-Platais, V., Dulude, M., Dahlen, T., Cox, C., 2012, WFC3 Instrument Science Report, WFC3-ISR-2012-07,(Baltimore:STScI)

Kozhurina-Platais, V., Hammer, D., Dencheva, N., Hack, W., 2013, WFC3 Instrument Science Report, WFC3-ISR-2013-14, (Baltimore:STScI)

Kozhurina-Platais, V.,2014, WFC3 Instrument Science Report, WFC3-ISR-2014-12, (Baltimore:STScI)

van der Marel, R., Anderson, J., Cox, C., Kozhurina-Platais, V., Lallo, M., Nelan, E., 2007, ACS Instrument Science Report, ACS-ISR-2007-07, (Baltimore:STScI)

Meurer, G., Lindler, D., Blakeslee, J., Cox, C., Martel, A., Tran, H., Bouwens, R., Ford, H., *et al.*, 2002,in "2002 HST Calibration Workshop", eds A.Arribas, A. Koekemoer, B.C, Whitmore (Baltimore:STScI), p.65

McArthur, B., 2014, (private communication)

van de Kamp, P., 1967, "Principles of Astrometry", by W. H. Freeman & Company (San Francisco and London)

Ubeda, L., Kozhurina-Platais, V., Bedin, L., 2013, ACS Instrument Scinece Report, ACS-ISR-2013-03,(Baltimore:STScI)